2021

Effects of anharmonicity in a Dual-Sagnac interferometer

Stephen Thomas
Georgia Southern University

Effects of anharmonicity in a Dual-Sagnac interferometer

An Honors Thesis submitted in partial fulfillment of the requirements for Honors in the Department of Physics and Astronomy.

By
Stephen Thomas

Under the mentorship of Dr. Mark Edwards

ABSTRACT

A recent experiment implemented a dual Sagnac atom interferometer (AI) for rotation sensing using a Bose-Einstein condensate (BEC) confined in a TOP-trap potential. The BEC is split twice by laser light to create two pairs of counter-orbiting clouds in a lowest-order harmonic potential with each pair acting as a separate Sagnac interferometer. After one orbit the two overlapping cloud pairs are split again and the interference patterns are inferred from the population of atoms in the zero-momentum state. We have simulated the impact of the presence of anharmonic terms in the potential on the performance of the AI as measured in a recent experiment by using a variational approximation of the Gross-Pitaevskii equation (GPE) model. This model based on the Lagrangian Variational Method where the condensate pieces are represented by Gaussian clouds. We have compared the phase differences between the dual interferometers as computed in the model with that predicted by the action computed over the classical path for various types of anharmonic terms and for condensates of different sizes to assess the impact of these on the interferometer performance.

Thesis Mentor:_____

Dr. Mark Edwards

Honors Director:_____

Dr. Steven Engel

November 2021
Department of Physics and Astronomy
Honors College
Georgia Southern University

Acknowledgements

First and foremost, I would like to thank my research advisor, Dr. Mark Edwards, for his continuous support during this project. Furthermore, for the multiple years of engaging my learning outside the classroom and laying the foundation for me to be a successful physicist. I'd also like to thank my friends, partner, and family for their unbounded love and encouragement throughout my studies. Finally, I'd like to thank the Physics and Astronomy department as well as the Honors College at Georgia Southern University for the education and opportunities I've been provided with.

Contents

List of Figures

1 Introduction

Interference occurs in a system when two or more waves superpose to form a new wave. That resulting wave can be used to make measurements about the system and is most commonly used to detect small displacements. An early demonstration of interfering light sources came about in 1801 when Thomas Young brought a primitive example of the modern double–slit apparatus to the Royal Society of London. Young also paralleled this presentation with an analogy for sound waves and water waves; however at the time, the wave theory of light contradicted the current held particle, or corpuscular, view developed by Newton in their 1704 publication *Opticks*. Throughout the 19^{th} century evidence for waves grew and in 1865 Maxwell published their *A Dynamical Theory of the Electromagnetic Field*. In which, the familiar electric and magnetic properties of the time were nicely described by a set of four equations. These equations also supported the idea that light could be treated as a wave in the electromagnetic field. In the early 20^{th} century the development of quantum mechanics and related experiments provided evidence for an intrinsic wave behavior of particles and matter. Presently, the usage of waves in interferometry is very wide spread through fields such as: astronomy, oceanography, spectroscopy, quantum systems, and many more! Electromagnetic waves offer the widest range of probing techniques due to the vast spectrum of wavelengths available, but the high energy radiation needed for probing smaller distance scales isn't always desirable. Quantum systems provide a feasible alternative for making precision measurements. One such quantum system is a gas of ultra–cold atoms in atom interferometers. Ultra–cold atom interferometry technology has developed significantly over the past 25 years [1] for various applications such as precision metrology [2–10], quantum sensing [11–22], and tests of fundamental physics [23–38]. Precision metrology includes applications such as measuring fundamental constants and the local acceleration of gravity as part of the new Kibble–balance kilogram standard. Quantum sensors are being developed to measure rotation and accelerations for use in precision navigation and civil engineering. Finally, these interferometer devices are used to search for dark–matter and dark–energy, as well as in testing Einstein's Equivalence Principle.

This work focuses on the atom interferometry device developed by a research group at the University of Virginia (UVa) which utilizes the Sagnac effect to measure the external rotation speed of the system [22,39–42]. We analyze the operation of the device using a recently developed variational model approximation to the standard mean–field theory given by the time–dependent Gross–Pitaesvkii equation. The model provides rapid approximate solutions under extreme conditions, such as the large–volume of the UVa device, and is developed for usage in any arbitrary power–law potential. Here it's used to investigate the effects of anharmonicty in the potential

for the UVa rotation sensor, as well as the effects of interactions due to increasing number of condensate atoms. Section [2] provides an overview of relevant background information and discusses how the Sagnac effect can be used to measure the rotation speed. Section [3] details the atom interferometry device developed by the UVa group and describes experimental procedure. Section [4] presents the approximation model and gives the equations of motion for any arbitrary power–law potential. This section also derives a formula for computing the rotation speed of the system. Section [5] discusses the simulations conducted and analyzes the effects of anharmonicity and interactions in the results. Finally, section [6] summarizes the work.

2 Background Information

The development of quantum mechanics in the 20th century has led to a realization of highly sensitive systems which can be used to probe the smallest structures of nature. It uses mathematical waves, known as wavefunctions, representing probability distributions to describe these systems and benefits from the well understood principles of interferometry. Bose–Einstein condensates, an ultra–cold gas of bosonic atoms, are one such quantum system.

2.1 Bose-Einstein Condensates

Louis Debroglie postulated in 1924 that all matter acts like a wave, at a small enough resolution scale. This matter-wave has a wavelength which is inversely proportional to its momentum, namely $\lambda = \frac{h}{p}$. Therefore, as the momentum decreases the spatial wavelength should increase. Albert Einstein, based on the work of Satyendranath Bose, realized that bosons could form a collection of identical particles governed by a single-particle wavefunction; originally realized for light by Bose, this could also occur for bosonic atoms if we cooled them down to nearly absolute zero in a small volume. As the temperature decreases, so does the velocity and thus the momentum. Since these are atoms with an integer total spin they don't obey the Pauli exclusion principle and can occupy the same ground state. At a critical temperature, $T_c \approx 10^1 - 10^2 nK$, the condensate begins to form in the highest density regions, $\rho \approx 10^{14}\ atoms/cm^3$, and the rest of the atoms quickly follow suit. At this point, the Debroglie wavelength is on the order of the spacing between the atoms in the gas, and they are indistinguishable from each other. The collection of atoms can be described by one single–particle wavefunction and have formed a Bose–Einstein condensates (BEC). Because of their collective quantum behavior, BECs offer an unprecedented scale at which to investigate the dynamics of the quantum mechanics. The wavefunctions describing these BECs are governed by a non–linear second order differential equation known as the Gross–Pitaesvkii equation, discussed next.

2.1.1 Derivation of the Gross-Pitaevskii Equation

BECs can be described by the time-dependent many-body Schrodinger equation,

$$i\hbar\frac{\partial}{\partial t}\Psi(\mathbf{r}_1,\ldots,\mathbf{r}_N,t) = \hat{\mathcal{H}}\Psi(\mathbf{r}_1,\ldots,\mathbf{r}_N,t) \tag{1}$$

where $\Psi(\mathbf{r}_1,\ldots,\mathbf{r}_N,t)$ is the many-body wavefunction describing a system of N particles, note that in general these particles will be interacting with each other. The i^{th} particle has coordinates denoted by the 3-tuple, $\mathbf{r}_i$, at time t. $\hat{\mathcal{H}}$ is the many-body Hamiltonian, a linear operator whose expectation value yields the total energy of the system. The energy of the system depends on

two terms, one due to the kinetic energy and the other due to any potential, external or internal. External potentials are able to be removed from the system, such as a magnetic field due to a set of coils. Internal potentials are intrinsic to the system and cannot be removed, in this case these arise from interactions of the many-bodies comprising the system. It's also critical to note that the solution, $\Psi(\mathbf{r}_1, \ldots, \mathbf{r}_N, t)$ must satisfy the normalization condition

$$\langle \Psi | \Psi \rangle \equiv \int_{-\infty}^{\infty} d^3 r_1 \cdots \int_{-\infty}^{\infty} d^3 r_N \Psi^*(\mathbf{r}_1, \ldots, \mathbf{r}_N, t) \Psi(\mathbf{r}_1, \ldots, \mathbf{r}_N, t) = 1 \tag{2}$$

where the integration is computed over all $3N$-dimensional space, and the asterisk superscript denotes complex conjugation of Ψ. This normalization condition ensures that the sum of the probabilities of all possible outcomes of a particular measurement will be equal to one.

The system in consideration for this work can be described as follows. All particles in the system are identical bosons of mass m. Bosons are particles with integer valued angular momentum, known as spin, and can occupy the same energy state. This is a consequence of the fact that bosons are described by symmetric wavefunctions. That is, a wavefunction which is unchanged when the positions of any two particles are swapped.

$$\Psi(\ldots, \mathbf{r}_i, \mathbf{r}_j, \ldots, \mathbf{r}_N, t) = \Psi(\ldots, \mathbf{r}_j, \mathbf{r}_i, \ldots, \mathbf{r}_N, t)$$

A wavefunction which becomes the negative of itself under such a swapping is anti-symmetric, and leads to inability for two particles, called fermions, to occupy the same energy state. It's key to note here that, in either case, these particles must be *indistinguishable* from one another, as is the case with N identical bosons.

The Hamiltonian for this system takes the form,

$$\hat{\mathcal{H}} = \sum_{i=1}^{N} \Big(\frac{-\hbar^2}{2m} \boldsymbol{\nabla}_i^2 + V(\mathbf{r}_i) \Big) + g \sum_{i<j}^{N} \delta(\mathbf{r}_i - \mathbf{r}_j) \tag{3}$$

where $\hbar = 1.055 \times 10^{-}34\ J\dot{s}$ is the reduced Planck's constant. This Hamiltonian is comprised of single particle operators which act on the i-th particle, $\frac{-\hbar^2}{2m} \boldsymbol{\nabla}_k^2$ and $V(\mathbf{r}_i)$, and a sum over distinct interacting pairs (i, j).

The interaction of the many-bodies is handled by a mean field approach in which the interaction with $N-1$ other particles is reduced to an interaction with an average field. The interacting identical particles setup a zero-range pseudo-potential, $V_{pseudo}(\mathbf{r}) = g\delta(\mathbf{r}_k - \mathbf{r_j}) = \frac{\mathbf{4}\pi\hbar^2\mathbf{a_s}}{\mathbf{m}} \delta(\mathbf{r_k} - \mathbf{r_j})$, the details of which are outlined in many books on the subject, for instance [43]. The interaction effects are assumed to be entirely due to 'contact' forces in two-body collisions and

are characterized by the mean field energy $g = \frac{4\pi\hbar^2 a}{m}$ which a particle experiences from $N-1$ other particles, where a is the scattering length. This pseudo-potential is valid largely due to two assumptions. The first being that the average distance between particles is always much larger than the scattering length a_s, known as the dilute limit for the gas. The other arises from the fact that these collisions take place at low energy. At these energies, the de-Broglie wavelength is on the order of the spacing between atoms. Hence any particle will not resolve the structure of the object it collides with and scatter with equal probability in every direction as a spherical outgoing wave, denoted the s-wave (because this state has angular momentum quantum number $l = 0$ as with s-orbitals in atoms).

In general, we cannot solve Eq.[1] exactly for the many-body wavefunction; however, we can find stationary approximate ground state solutions using an ansatz. Stationary solutions are the solutions to the time-independent Schrodinger equation

$$\hat{\mathcal{H}} \left|\phi\right\rangle = E_\phi \left|\phi\right\rangle$$

and correspond to a state with a single definite energy. The state can still evolve through time via a complex phase factor, but the probability distribution and expectation value associated to any observable are constant through time. This process of finding these solutions applies variational principles to quantum mechanics with an assumed trial wavefunction which is the symmetrized product of single-particle wave functions, an assumption known as the Hartree-Fock approximation. In the fully condensed state (zero temperature), all the bosons can occupy the same ground state described by the single-particle state, $\phi(\mathbf{r})$. Therefore we can write the many-body wavefunction Ψ as follows,

$$\Psi(\mathbf{r}_1, \ldots, \mathbf{r}_N) = \prod_{i''=1}^{N} \phi(\mathbf{r}_{i''}) \tag{4}$$

where the time-dependent version is given by plugging the single-particle wavefunction, $\phi(\mathbf{r})$, into the time-dependent Schrodinger equation. The result of which is

$$i\hbar \frac{\partial}{\partial t} \left|\phi(t)\right\rangle = \hat{\mathcal{H}} \left|\phi(t)\right\rangle = E_\phi \left|\phi(t)\right\rangle$$

a differential equation whose solution is

$$\left|\phi(t)\right\rangle = e^{-i\frac{E_\phi t}{\hbar}} \left|\phi(t=0)\right\rangle .$$

This allows one to write the time-dependent trial wavefunction as follows,

$$\Psi(\mathbf{r}_1,\ldots,\mathbf{r}_N,t) = e^{-i\frac{E_\phi t}{\hbar}} \prod_{i''=1}^{N} \phi(\mathbf{r}_{i''}) \tag{5}$$

To determine the energy of this state, E, we need to calculate the expectation value of the many-body Hamiltonian, which will yield the average value of the energy of this state. This can be done as follows, (where $\int_{-\infty}^{\infty} d^3R = \prod_{k=1}^{N}\int_{-\infty}^{\infty} d^3r_k$, is the integral over all spatial-coordinates of the wavefunction)

$$\begin{aligned}
E[\phi^*] = \langle\mathcal{H}\rangle &= \langle\Psi|\,\hat{\mathcal{H}}\,|\Psi\rangle \\
&= \int_{-\infty}^{\infty} d^3R\ \Psi^*\hat{\mathcal{H}}\Psi \\
&= \int_{-\infty}^{\infty} d^3R\ (e^{i\frac{E_\phi t}{\hbar}} \prod_{i'=1}^{N} \phi^*(\mathbf{r}_{i'}))\hat{\mathcal{H}}(e^{-i\frac{E_\phi t}{\hbar}} \prod_{i''=1}^{N} \phi(\mathbf{r}_{i''})) \\
&= \int_{-\infty}^{\infty} d^3R\ (\prod_{i'=1}^{N} \phi^*(\mathbf{r}_{i'}))\left[\sum_{i=1}^{N}\Big(\frac{-\hbar^2}{2m}\boldsymbol{\nabla}_i^2 + V(\mathbf{r}_i)\Big) + g\sum_{i<j}^{N}\delta(\mathbf{r}_i-\mathbf{r}_j)\right](\prod_{i''=1}^{N} \phi(\mathbf{r}_{i''})) \\
&= \int_{-\infty}^{\infty} d^3R\ (\prod_{i'=1}^{N} \phi^*(\mathbf{r}_{i'}))\left[\sum_{i=1}^{N}\Big(\frac{-\hbar^2}{2m}\boldsymbol{\nabla}_i^2 + V(\mathbf{r}_i)\Big)\right](\prod_{i''=1}^{N} \phi(\mathbf{r}_{i''})) \\
&\quad + \int_{-\infty}^{\infty} d^3R(\prod_{i'=1}^{N} \phi^*(\mathbf{r}_{i'}))\left[g\sum_{i<j}^{N}\delta(\mathbf{r}_i-\mathbf{r}_j)\right](\prod_{i''=1}^{N} \phi(\mathbf{r}_{i''}))
\end{aligned} \tag{6}$$

We can separate off the wavefunctions not included in the sums which yields,

$$\begin{aligned}
E[\phi^*] = &\int_{-\infty}^{\infty} d^3R\ \sum_{i=1}^{N}\left(\prod_{i'\neq i}^{N}\phi^*(\mathbf{r}_{i'})\phi(\mathbf{r}_{i'})\right)\phi^*(\mathbf{r}_i)\Big(\frac{-\hbar^2}{2m}\boldsymbol{\nabla}_i^2 + V(\mathbf{r}_i)\Big)\phi(\mathbf{r}_i) \\
&+ g\int_{-\infty}^{\infty} d^3R\sum_{i<j}^{N}\left(\prod_{i'\neq i\neq j}^{N}\phi^*(\mathbf{r}_{i'})\phi(\mathbf{r}_{i'})\right)\phi^*(\mathbf{r}_i)\phi^*(\mathbf{r}_j)\delta(\mathbf{r}_i-\mathbf{r}_j)\phi(\mathbf{r}_i)\phi(\mathbf{r}_j)
\end{aligned} \tag{7}$$

Utilizing the normalization condition given by Eq. (2) and the properties of the Dirac delta-function, we have

$$E[\phi^*] = \sum_{i=1}^{N}\int_{-\infty}^{\infty} d^3r_i\ \phi^*(\mathbf{r}_i)\Big(\frac{-\hbar^2}{2m}\boldsymbol{\nabla}_i^2 + V(\mathbf{r}_i)\Big)\phi(\mathbf{r}_i) + g\sum_{i<j}^{N}\int_{-\infty}^{\infty} d^3r_i\phi^*(\mathbf{r}_i)\phi^*(\mathbf{r}_i)\phi(\mathbf{r}_i)\phi(\mathbf{r}_i) \tag{8}$$

Finally, since all the particles have the same wavefunction we can replace the sums with N and

$\frac{N(N-1)}{2}$ respectively, so that,

$$E[\phi^*] = N\int_{-\infty}^{\infty} d^3r\ \left[\phi^*(\mathbf{r})\Big(\frac{-\hbar^2}{2m}\boldsymbol{\nabla}^2 + V(\mathbf{r})\Big)\phi(\mathbf{r}) + g\frac{N-1}{2}\phi^{*2}(\mathbf{r})\phi^2(\mathbf{r})\right] \tag{9}$$

Equation (9) is the energy functional which yields the energy of the single particle state ϕ^*. In order to determine the ground state solution we seek to minimize the energy functional with respect to independent variations of $\phi^*(\mathbf{r})$, or its complex conjugate $\phi(\mathbf{r})$, along with the additional constraint that the solution must satisfy

$$\langle\phi^*|\phi^*\rangle \equiv \int_{-\infty}^{\infty} d^3r\ \phi^*(\mathbf{r})\phi(\mathbf{r}) = 1 \implies \int_{-\infty}^{\infty} d^3r\ \phi^*(\mathbf{r})\phi(\mathbf{r}) - 1 = 0$$

This can be carried out by the use of Lagrange multipliers. In doing so we wish to find a solution, ϕ, which yields a stationary value of

$$\mathcal{L}(\mathbf{r},\lambda) = E[\phi^*] - \lambda G[\phi^*] \tag{10}$$

This is accomplished by letting ϕ^* vary (denoted $\delta\phi^*$), and forcing the first variation to vanish as follows

$$\begin{aligned}
0 &= (E[\phi^* + \delta\phi^*] - E[\phi^*]) - \lambda(G[\phi^* + \delta\phi^*] - G[\phi^*]) \\
&= \Bigg(N\int_{-\infty}^{\infty} d^3r\ \Big(\phi^*(\mathbf{r}) + \delta\phi^*(\mathbf{r})\Big)\Big(\frac{-\hbar^2}{2m}\boldsymbol{\nabla}^2 + V(\mathbf{r})\Big)\phi(\mathbf{r}) \\
&+ \quad g\frac{N-1}{2}\Big(\phi^*(\mathbf{r}) + \delta\phi^*(\mathbf{r})\Big)^2\phi^2(\mathbf{r}) \\
&- \quad N\int_{-\infty}^{\infty} d^3r\ \phi^*(\mathbf{r})\Big(\frac{-\hbar^2}{2m}\boldsymbol{\nabla}^2 + V(\mathbf{r})\Big)\phi(\mathbf{r}) + g\frac{N-1}{2}\phi^{*2}(\mathbf{r})\phi^2(\mathbf{r})\Bigg) \\
&- \quad \lambda\Bigg(\int_{-\infty}^{\infty} d^3r\ \Big(\phi^*(\mathbf{r}) + \delta\phi^*(\mathbf{r})\Big)\phi(\mathbf{r}) - 1 - \Big(\int_{-\infty}^{\infty} d^3r\ \phi^*(\mathbf{r})\phi(\mathbf{r}) - 1\Big)\Bigg)
\end{aligned} \tag{11}$$

After some simplifications (noting that $\phi^*\phi = |\phi|^2$), and keeping only the terms which are linear in $\delta\phi^*$, we arrive at

$$\int_{-\infty}^{\infty} d^3r\ \delta\phi^*\Big[N\Big((\frac{-\hbar^2}{2m}\boldsymbol{\nabla}^2 + V(\mathbf{r})) + g(N-1)|\phi|^2\Big)\phi - \lambda\phi\Big] = 0 \tag{12}$$

Since the variations, $\delta\phi^*$, are arbitrary, we can conclude that $\phi(\mathbf{r})$ must satisfy the equation

$$\Big(\frac{-\hbar^2}{2m}\boldsymbol{\nabla}^2 + V(\mathbf{r}) + g(N-1)|\phi|^2\Big)\phi = \mu\phi \tag{13}$$

Equation (13) is known as the time-independent Gross-Pitaevskii equation (GPE), where $\mu = \frac{\lambda}{N}$ is still unknown. The factor of $N-1$ appears as we've assumed there to be a definite number of condensate atoms, N. An equation for μ can be found by multiplying (on the left) the GPE by ϕ^* and then integrating over all space, which yields,

$$\mu = \int_{-\infty}^{\infty} d^3r \left(\phi^*(\frac{-\hbar^2}{2m}\boldsymbol{\nabla}^2 + V(\mathbf{r}))\phi + g(N-1)|\phi|^4\right) \tag{14}$$

Given the energy functional in Eq.(9) and the first law of thermodynamics (where the entropy and volume are fixed, $dS = 0$ and $dV = 0$), the chemical potential $\partial E/\partial N$ can be computed as follows

$$\frac{\partial E}{\partial N} = \int_{-\infty}^{\infty} d^3r \Big(\phi^*(\frac{-\hbar^2}{2m}\boldsymbol{\nabla}^2 + V(\mathbf{r}))\phi + g(N-1/2)|\phi|^4\Big) \tag{15}$$

which in the limit that $N >> 1$ we can see that Eq.(14) and Eq.(15) are the exact same. Therefore, in this limit, we can interpret μ as the chemical potential of the condensate, $\mu = \frac{\partial E}{\partial N}$. This is the amount of energy required to add another particle to the condensate.

Given an external potential $V(\mathbf{r})$, the solutions to the time-independent GPE, where the chemical potential is given by Eq.(15), yield an equilibrium mean field approximate form of the single-particle wavefunction that all the particles in the system share.

A time-dependent GPE can be determined using the variational principle for the action (ref pethick). The action principle states that the solutions to the equations of motion describing the system must be stationary points of the action functional, S, given by,

$$S[\mathbf{q}(t)] = \int_{t_1}^{t_2} L(\mathbf{q}(t), \dot{\mathbf{q}}(t), t)dt \tag{16}$$

where $\mathbf{q}(t)$ is an n-tuple containing the generalized coordinates $\{q_i(t)\}$ and $\dot{\mathbf{q}}(t)$ is an n-tuple containing their derivatives with respect to the independent parameter t, where t is time and n the number of degrees of freedom of the system. Stationary points are ones for which the variation of the action, δS, is zero to first order approximations of small variations in the solution. These variations are arbitrary and require that they vanish at the temporal boundaries, t_1 and t_2. The Euler Lagrange equations can be determined by allowing the generalized coordinates to vary arbitrarily small to first order. That is $g_\epsilon(t) = q(t) + \epsilon\eta(t)$ where ϵ is arbitrarily small, and $\eta(t_1) = \eta(t_2) = 0$. After further work, one can find the generalized coordinates must satisfy the following equations,

$$\frac{d}{dt}(\frac{\partial L}{\partial \dot{q}_i}) - \frac{\partial L}{\partial q_i} = 0, \quad i = 1, \ldots, n \tag{17}$$

This description needs to be modified slightly for it's usage in quantum field theory, as is the case with BECs. In this case, a Lagrangian density used and the independent parameter, t, is replaced by an *event* in spacetime. Events are simply a name given to a point in spacetime specified by $s = (x, y, z, t)$. The dependent parameters, or generalized coordinates, are replaced by the value of a field at a point in spacetime, $\phi(x, y, z, t)$. Making these changes we can rewrite the action functional as follows

$$S[\phi_i] = \int \mathcal{L}(\phi_i(s), \{\frac{\partial \phi_i(s)}{\partial s^\alpha}\}, \{s^\alpha\}) d^4 s \tag{18}$$

where i denotes the functional for the $i-th$ field and $\alpha = \{1, 2, 3, 4\}$ indexes the variables of s. In the case of BECs we assume only a single scalar field, and hence we can write Eq.(18) as

$$S[\phi] = \int \mathcal{L}(\phi(s), \{\frac{\partial \phi(s)}{\partial \eta}, \frac{\partial \phi(s)}{\partial t}\}, \{\eta, t\}) d^3 r dt \tag{19}$$

where $\phi(x, y, z, t)$ is the solution we seek, and η and t are the independent parameters, with $\eta = x, y, z$ and $d^3 r = dxdydz$. Here the variations in ϕ must vanish at the temporal boundaries t_1 and t_2 as well as (for all time) any spatial boundaries.

The Lagrangian density used in this case (for $N >> 1$) is given as follows:

$$\begin{aligned} \mathcal{L}[\phi^*, \phi^*_\eta, \phi^*_t, \eta, t] &= \frac{i\hbar}{2}(\phi\phi^*_t - \phi^*\phi_t) + \Big[\frac{\hbar^2}{2m}|\boldsymbol{\nabla}\phi|^2 + V_{ext}(\mathbf{r}, t)|\phi|^2 \frac{1}{2} g N |\phi|^4\Big] \\ &= \frac{i\hbar}{2}(\phi\phi^*_t - \phi^*\phi_t) + \mathcal{E} \end{aligned} \tag{20}$$

where $\phi_\eta \equiv \frac{\partial \phi}{\partial \eta}$, $\phi_t \equiv \frac{\partial \phi}{\partial t}$, and the term $\mathcal{E}$ is the energy density. This Lagrangian density, along with the following Euler-Lagrange equation allows one to derive the time-dependent GPE,

$$\sum_{\eta = x,y,z,t} \frac{\partial}{\partial \eta}\Big(\frac{\partial \mathcal{L}}{\partial \phi^*_\eta}\Big) - \frac{\partial \mathcal{L}}{\partial \phi^*} = 0 \tag{21}$$

where

$$\phi^*_t \equiv \frac{\partial \phi^*}{\partial t} \quad \text{and} \quad \phi^*_\eta \equiv \frac{\partial \phi^*}{\partial \eta}$$

The derivatives in Eq.(21) are as follows,

$$\begin{aligned}
\frac{\partial \mathcal{L}}{\partial \phi_x^*} &= \frac{\hbar^2}{2m}\phi_x \\
\frac{\partial \mathcal{L}}{\partial \phi_y^*} &= \frac{\hbar^2}{2m}\phi_y \\
\frac{\partial \mathcal{L}}{\partial \phi_z^*} &= \frac{\hbar^2}{2m}\phi_z \\
\frac{\partial \mathcal{L}}{\partial \phi_t^*} &= \frac{i\hbar}{2}\phi \\
\frac{\partial \mathcal{L}}{\partial \phi^*} &= -\frac{i\hbar}{2}\phi_t + V_{ext}(\mathbf{r},t)\phi + gN|\phi|^2\phi
\end{aligned}$$

so then we can rewrite the Euler Lagrange equation as follows,

$$\frac{\partial}{\partial x}(\frac{\hbar^2}{2m}\phi_x) + \frac{\partial}{\partial y}(\frac{\hbar^2}{2m}\phi_y) + \frac{\partial}{\partial z}(\frac{\hbar^2}{2m}\phi_z) + \frac{\partial}{\partial t}(\frac{i\hbar}{2}\phi) + \frac{i\hbar}{2}\phi_t - V_{ext}(\mathbf{r},t)\phi - gN|\phi|^2\phi = 0$$

finally arriving at,

$$i\hbar\frac{\partial}{\partial t}\phi(x,y,z,t) = \Big(-\frac{\hbar^2}{2m}\nabla^2 + V_{ext}(\mathbf{r},t) + gN|\phi|^2\Big)\phi(x,y,z,t) \tag{22}$$

where Eq.(22) is the standard time-dependent Gross-Pitaevskii equation with: $\phi(x,y,z,t)$ the single particle wavefunction, m the mass of a condensate atom, N the number of condensate atoms, $g = 4\pi\hbar^2 a_s/m$ is a parameter governing the strength of atom-atom scattering, where a_s is the s-wave scattering length, and V_{ext} is the external potential.

The GPE can also be derived in a rotating reference frame by a transformation of coordinate systems. By doing so, one arrives at the rotating frame GPE (RGPE),

$$\begin{aligned}
i\hbar\frac{\partial}{\partial t}\psi(\mathbf{r},t) = &-\frac{\hbar^2}{2M}\nabla^2\psi(\mathbf{r},t) + V_{\text{ext}}(\mathbf{r},t)\psi(\mathbf{r},t) + gN\left|\psi(\mathbf{r},t)\right|^2\psi(\mathbf{r},t) \\
&+ \quad i\hbar\boldsymbol{\Omega}\cdot(\mathbf{r}\times\nabla)\,\psi(\mathbf{r},t)
\end{aligned} \tag{23}$$

which has an additional term present that is dependent on the rotation speed, Ω.

2.1.2 Solutions of the GPE

Exact solutions of the GPE are not generally known nor easily found, and instead a numerical computation approach, such as the split–step Crank–Nicolson method, is used. To simulate the behavior of the condensates the value of the wavefunction is calculated at each point in the space and this process is iterated through time. The non-linear term due to interactions appearing in the GPE makes accurate computational solutions difficult, requiring considerable memory space and run time. Due to the computational capacity, this significantly limits the conditions which

can be investigated accurately and in a reasonable amount of time. To investigate more extreme conditions, such as when the condensates are separated by large distances as compared to their size or when there are multiple clouds with large momenta, an approximation method is needed. This is discussed in section [4], Lagrangian Variational Method.

2.1.3 Condensate Phase

Experiments in atom interferometry can often be treated using Feynman's path integral approach to quantum mechanics as demonstrated by Storey and Cohen–Tannoudji. They show that the phase of the wavefunction can be determined by the action along the trajectory taken by a classical particle. To determine the wavefunction at any subsequent position we need only the initial conditions and to consider the action along the classical path. This is very powerful as it reduces the computational process to evaluating integrals along classical paths, but it is also limited. Storey and Cohen–Tannoudji outline several applications of this process to atom interferometry systems. These include: a free particle, a two-level atom crossing a laser wave, a particle in a gravitational field, a particle in a rotating frame, and the atomic equivalents of the Aharonov-Bohm effects. These systems all share the benefit of a quadratic Lagrangian which is fairly easy to compute a path integral for. However, in reality quadratic Lagrangians are often approximations for the system and ignore higher order terms. In precision measurement system it is necessary to consider these higher order terms and hence a different approach to determining the evolution of the wavefunction must be used.

2.2 Atom Interferometry

Because of the wave nature of quantum mechanics, BEC's can interfere with each other and these interference patterns can be used to extract information about the system. Interference patterns occur when two, or more, waves overlap. These can be any kind of wave from mechanical to electromagnetic, or even gravitational. Consider two waves of the same energy; when overlapping, the amplitude of these waves will sum up to a new wave which is the result of superposing the constituent waves. The resulting amplitude depends on the phase difference between the two waves. A maximum amplitude occurs when they are in phase with each other, and a minimum when they are 180° out of phase. The phase of the wave depends on spatial and temporal parameters such as position and frequency; because of this, the phase can be used to extract information about the environment of the wave. Interferometry utilizes the interference patterns between overlapping waves to make measurements. Typical interferometer devices use electromagnetic waves from lasers to interfere, but recent technologies have provided the capability to manipulate atoms with lasers at a very precise level. Because of this, ultra-cold atom

interferometer systems are possible. Interferometer devices are already widely in use across the world and in space, in areas such as precision navigation and remote sensing. Atom interferometers offer a benefit to current systems by correcting for the measurement drifts in laser based ones. Sagnac interferometers are already widely in use in inertial navigation systems with lasers, but the use of atom interferometers offers a much greater sensitivity due to the slower motion of the atoms as compared to light

2.2.1 Sagnac Interferometer

A particular type of interferometer, known as a Sagnac interferometer is used in the rotation sensor being developed by the research group at UVa. The Sagnac effect occurs due to split waves travelling along a common–path in opposite directions while in a rotating system. The rotation causes a spatial phase shift as one wave travels in the direction of rotation and the other against. When the waves re–overlap along the path the resulting amplitude depends on the phase difference between them, which in turn depends on the rotation speed. The UVa rotation sensor uses a dual-Sagnac interferometer with Bose–Einstein condensates. It achieves this by starting with two waves, on opposite sides of a circular path, each split into their own pair forming two independent Sagnac interferometers. Each one has an associated phase difference between the clouds in that interferometer. This phase difference is subject to noise from the environment such as mechanical vibrations in the device or ambient magnetic fields; anything which perturbs the energy of the system. With two interferometers, the difference between the top and bottom interferometer measurements provides the experimental benefit of removing phase contributions from common-mode noise sources while the oppositely signed Sagnac phases will add up.

The clouds in a pair will have oppositely oriented angular momentum. Therefore, upon calculating the difference in the action over their respective classical paths, one finds the resulting phase difference between clouds in a pair is dependent only on the rotation of the apparatus with respect to an inertial reference frame.

$$\Phi_S = \frac{1}{\hbar} \oint \Delta L \cdot \Omega dt = \frac{4M\Omega A}{\hbar} \tag{24}$$

where Φ_S is the phase difference between a pair of clouds due to the Sagnac effect, ΔL is difference in angular momentum between the clouds, A the area subtended by the classical path, and Ω is the rotation speed in reference to the rest frame. This rotation is about an axis perpendicular to the area enclosed by the paths. Furthermore, the Sagnac phase in the top and bottom interferometers have opposite signs. Thus the phase difference between the top and bottom interferometers is

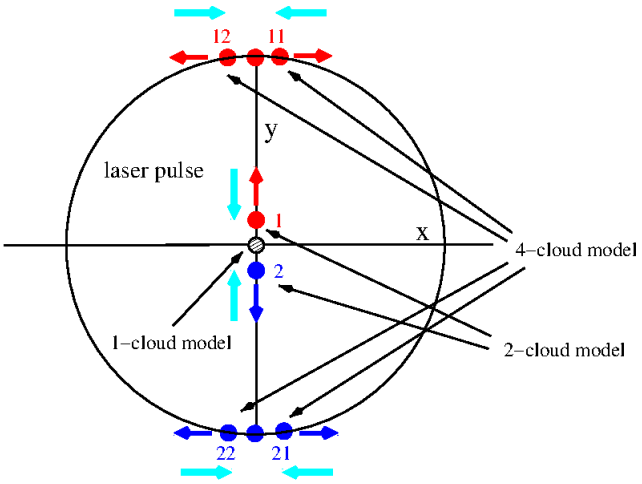

Figure 1: The Virginia dual Sagnac interferometer sequence as viewed from a non–rotating frame. A BEC (gray circle) is formed in an ideally harmonic trap ($\omega_x = \omega_y \equiv \omega_\perp$) at the trap center. **First Split:** laser pulses are used to split the BEC into two clouds that move at speed v_B along the $+y$ axis (cloud 1) and the $-y$ axis (cloud 2), respectively. **Second Split:** At time $t = t_1$ cloud 1 at the top is split into clouds 11 and 12. Cloud 11 has a $+v_B\hat{\mathbf{i}}$ added to its velocity by the split while cloud 12 has $-v_B\hat{\mathbf{i}}$ added. These clouds move around a circular orbit in opposite directions. Cloud 2 at the bottom is split into clouds 21 and 22 that also orbit oppositely. **Final split:** both of these cloud pairs are allowed to execute one orbit and, at time $t = t_2$, when each pair of clouds re–overlaps they are split in the same way as the Second Split. Each re–overlapped pair is split into four clouds: two overlapping clouds that are nearly motionless and two that continue orbiting in opposite directions. Thus the (11,12) cloud pair form one Sagnac interferometer which we will call the "plus" (+) Sagnac interferometer and the (21,22) cloud pair forms the "minus" (-) Sagnac interferometer.

$$\Delta\Phi = \Phi_+ - \Phi_- = 2\Phi_S = \frac{8M\Omega A}{\hbar} \tag{25}$$

where Φ_+ and Φ_- are the phase differences in the top and bottom interferometers respectively.

It's worth restating here that this result relies on the rotation being treated as a perturbation to the Lagrangian and that the Lagrangian is quadratic. The accuracy of this model in the presence of the trapping potential used in the experiment at UVa is investigated in this work as the Lagrangian is not quadratic.

3 Dual-Sagnac Atom Interferometer

3.1 Operation

In the device designed by the UVa group, a ^{87}Rb, BEC containing around 10^4 atoms, in the ($F = 2$, $m_f = 2$) magnetic state, is formed initially at rest in the center of a cylindrically symmetric ideally harmonic potential, see the following figure 1. The condensate is manipulated via a standing wave double Bragg pulse which can split the clouds and provide a momentum

kick of $\mathbf{p} = \pm 2\hbar\mathbf{k}$, where $\mathbf{k}$ is the wavevector of the laser. The laser is reflected off of a mirror to form a standing wave. The laser is tuned to be slightly off resonant of the atomic energy levels, which as mentioned before pushes or pulls on the atoms. The first pulse places the atoms in an equal superposition of the ground and excited states in the momentum basis, $|0\rangle$ and $|+\rangle$, namely

$$|\psi\rangle = \frac{1}{\sqrt{2}}(|0\rangle + |+\rangle).$$

After allowing the phase to evolve, the second pulse is applied, changing the $|\psi\rangle = \frac{1}{\sqrt{2}}(|0\rangle - |+\rangle)$ to $|\psi\rangle = |+\rangle = \frac{1}{\sqrt{2}}(|v_B\rangle + |-v_B\rangle)$, detailed in Refs. [41], [44]. Overall, this splits the cloud into two with opposite momenta, expressed by the resultant velocity as $v_B = \pm\frac{2\hbar k}{m}$. The first applied double Bragg pulse splits the initial condensate along the $\pm\hat{\mathbf{y}}$ direction. The two clouds then move according to $x(t) = 0$ and $y_{1,2}(t) = \pm R\sin(\omega t) = \pm v_B/\omega \sin(\omega t)$. They reach the classical turning point, $R = v_B/\omega$, at a time $t_1 = \frac{1}{4}T_{trap} = \pi/(2\omega)$. At this point, another double Bragg pulse along the $\pm\hat{\mathbf{x}}$ direction is applied to each cloud, splitting them into two pairs, a total of four clouds. Each pair of clouds moves according to $x(t) = \pm R\sin(\omega t)$ and $y(t) = \pm R\cos(\omega t)$ and complete an orbit after one trap period, namely $t_2 = T_{trap} = 2\pi/\omega$. Once completing an orbit, a final double Bragg pulse, in the $\pm\hat{\mathbf{x}}$ direction, is applied coupling the even state $|\psi\rangle = \frac{1}{\sqrt{2}}(|v_B\rangle + |-v_B\rangle)$ to $|0\rangle$, the odd state $|\psi\rangle = \frac{1}{\sqrt{2}}(|v_B\rangle - |-v_B\rangle)$ remains unchanged up to an overall phase. Prior to this final pulse, the wavefunction of a pair of clouds can be expressed as

$$|\Psi\rangle = \frac{1}{\sqrt{2}}(e^{i\Phi/2}|v_B\rangle + e^{-i\Phi/2}|-v_B\rangle) \tag{26}$$

where Φ is the phase difference between clouds in an interferometer. Projecting this onto the even superposition state we have,

$$\begin{aligned}
\frac{1}{\sqrt{2}}(\langle v_B| + \langle -v_B|)|\Psi\rangle &= \frac{1}{2}e^{i\Phi/2} + \frac{1}{2}e^{-i\Phi/2} \\
&= \frac{1}{2}(\cos(\Phi/2) + i\sin(\Phi/2) + \cos(-\Phi/2) + i\sin(-\Phi/2)) \\
&= \frac{1}{2}(\cos(\Phi/2) + i\sin(\Phi/2) + \cos(\Phi/2) - i\sin(\Phi/2)) \\
&= \frac{1}{2}(2\cos(\Phi/2))
\end{aligned}$$

with probability

$$\begin{aligned}
|(\langle v_B| + \langle -v_B|)|\Psi\rangle|^2 &= |(\cos(\Phi/2))|^2 \\
S &= \cos^2(\Phi/2)
\end{aligned}$$

This result shows that the probability, S, of being in the zero momentum state after the final pulse is proportional to the rotation speed of the system. The probability is also equal to the fraction of stopped atoms, which is measured using absorption imaging. The result of which is a fraction of stopped atoms for the top interferometer, S_+, and for the bottom interferometer, S_-. In the experiment, this process is repeated and the rotation speed of the system is determined by plotting multiple results of measuring S_+ and S_- against each other. This data can then be fit to an ellipse from which the phase difference between the top, +, and bottom, -, interferometers can be determined [45].

$$\Delta\Phi_\pm = \Delta\Phi_+ - \Delta\Phi_-. \tag{27}$$

In this way common-mode noise sources are subtracted out while the Sagnac phase contributions add since they affect the two interferometers oppositely. There are no noise sources in the simulations so we can determine $\Delta\Phi_\pm$ for each interferometer separately with no need for ellipse fitting.

3.2 TOP Trap and Anharmonicity

The condensate is confined by magnetic fields with a time-orbiting potential, known as a TOP trap. It consists of a rotating bias field and a rotating quadrupole field. These fields are setup by six independent coils placed on the surface of a cube, designed by Horne *et Al.* in Ref. [40]. The rotating bias field can be expressed as follows,

$$\mathbf{B}_0 = B_0\Big[(1+\alpha)\sin(\Omega_1 t)\cos(\Omega_2 t+\beta)\hat{\mathbf{x}} + (1-\alpha)\sin(\Omega_1 t)\sin(\Omega_2 t-\beta)\hat{\mathbf{y}} + \cos(\Omega_1 t)\hat{\mathbf{z}}\Big] \tag{28}$$

where $\Omega_1 \approx 2\pi \times 10^4 Hz$ and $\Omega_2 \approx 2\pi \times 10^3 Hz$. By default, α and β, the amplitude and phase asymmetry, are zero; but they can be adjusted to optimize the trap.

The rotating quadrupole field takes the form,

$$\mathbf{B}_q = \frac{1}{2}B_1' \cos(\Omega_1 t)(x\hat{\mathbf{x}} + y\hat{\mathbf{y}} - 2z\hat{\mathbf{z}}) \tag{29}$$

where $B_1' = \frac{2mg}{\mu_B} \approx 31\frac{G}{cm}$ is the magnitude of the quadrupole gradient along the z axis.

These fields oscillate synchronously with each other such that there is an upwards force at the center of the trap, set to cancel gravity. The zero of the quadrupole is also displaced and orbits around the center. This helps prevent ejections due to Majorana spin flips, a non-adiabatic transition of the atoms to an inverted spin orientation. The inversion results in those atoms experiencing an anti-trapping potential and thus they are ejected. This typically happens as the

atoms reach the zeros of the magnetic fields, as discussed in Ref. [46]. The spin flip is also likely to occur if the rotation of the bias field is faster than the precession of the atom's magnetic dipole, known as the Larmor frequency. Therefore the rotation rate of the bias field is slow relative to the Larmor frequency but fast relative to the motional frequency of the atoms. Thus the atoms experience a time-averaged potential from the magnetic field,

$$V(\mathbf{r}) = \mu\langle|\mathbf{B}|\rangle \tag{30}$$

where $\langle|\mathbf{B}|\rangle$ is the time-average of the magnetic field magnitude. Given equations [1] and [2], the time-dependent magnitude of the magnetic field is as follows,

$$\begin{aligned} |\mathbf{B}|(t) &= |\mathbf{B}_0 + \mathbf{B}_q| \\ &= B_0[1 + \frac{1}{2}\kappa x \sin(2\Omega_1 t)\cos(\Omega_2 t) + \frac{1}{2}\kappa y \sin(2\Omega_1 t) \\ &\quad \sin(\Omega_2 t) - 2\kappa z \sin^2(\Omega_1 t) + \frac{1}{4}\kappa^2(\rho^2 + 4z^2)\sin^2(\Omega_1 t)]^{1/2} \end{aligned} \tag{31}$$

where $\kappa \equiv B_1/B_0$ and $\rho^2 = x^2 + y^2$.

Taylor expanding the square root to fourth order in the quantities $(\kappa x, \kappa y, \kappa z)$ and subsequently averaging over time yields the following,

$$\begin{aligned} \langle|\mathbf{B}|\rangle = B_0[1 - \frac{1}{2}\kappa z + \frac{7}{128}\kappa^2\rho^2 + \frac{1}{16}\kappa^2 z^2 + \frac{1}{32}\kappa^3 z^3 \\ + \frac{9}{256}\kappa^3\rho^2 z - \frac{237}{131072}\kappa^4\rho^4 + \frac{17}{1024}\kappa^4 z^4 + \frac{93}{4096}\kappa^4\rho^2 z^2] \end{aligned} \tag{32}$$

Accounting for gravity in the vertical, z direction, the full potential can be expressed as follows,

$$V(\mathbf{r}) = \mu\langle|\mathbf{B}|\rangle + mgz$$

Then, setting $\mu B_0 \kappa = 2mg$ to place the potential minimum at the origin, the potential can be written as,

$$V(\mathbf{r}) = m\omega_0^2[\frac{1}{2}\rho^2 + \frac{\lambda^2}{2}z^2 + \frac{1}{3}az^3 + \frac{1}{2}b\rho^2 z + \frac{1}{4}c\rho^4 + \frac{1}{4}fz^4 + \frac{1}{2}h\rho^2 z^2] \tag{33}$$

where the horizontal frequency ω_0 is,

$$\omega_0 = (\frac{7}{64}\frac{\mu}{m}\frac{B_1^2}{B_0})^{1/2}$$

also the coefficients are,

$$\lambda^2 = \frac{8}{7} \quad a = \frac{6}{7}\kappa \quad b = \frac{9}{14}\kappa \quad c = -\frac{237}{3584}\kappa^2 \quad f = \frac{17}{28}\kappa^2 \quad h = \frac{93}{224}\kappa^2$$

The TOP trap used in this device has anharmonic contributions to the potential which can affect the condensates in an interferometer differently, introducing unwanted phase changes. For this reason, the potential is thoroughly analyzed to determine the anharmonicity of the trap and to find ways to minimize it. The experimental group at the University of Virginia have used a semi–classical approach to demonstrate the sensitivity of the device, however it requires considerable control over the trap parameters [47]. In the next section we describe an approximation method to the GPE and use this as an alternative approach for modeling the device. Ultimately this will provide a new method of extracting the rotation speed while also accounting for interactions and anharmonicity.

4 Lagrangian Variational Method

The variational model we developed is based on the Lagrangian Variational Method (LVM) and provides rapid approximations to the solutions of the Gross-Pitaevskii equation, which has the form given by Eq.(22). In our case we'll use the GPE in the rotating frame given by , denoted RGPE. The model assumes a trial wavefunction consisting of N_c number of 3-D Gaussian clouds which each have an associated initial momentum, $\mathbf{k}_j$, and set of variational parameters, $\{q(t)\}_j$, where j indexes the clouds. The equations of motion for these variational parameters are derived by integrating the Lagrangian density over all space yielding the ordinary Lagrangian; and then using the trial wavefunction and the standard Euler–Lagrange equations the equations can be found for each variational parameter associated to the j^{th} cloud, $q_j^i(t)$, where i indexes the set of variational parameters that each cloud has.

$$\begin{aligned} L(\{q(t)\}_j, \{\dot{q}(t)\}_j, t) &= \int_{-\infty}^{\infty} d^3r \mathcal{L}[\Psi, \Psi_\eta, \Psi_t, \eta, t] \\ &= \int_{-\infty}^{\infty} d^3r \Big[\frac{i\hbar}{2}(\Psi\Psi_t^* - \Psi^*\Psi_t) + \frac{\hbar^2}{2m}|\boldsymbol{\nabla}\Psi|^2 + V_{ext}(\mathbf{r},t)|\Psi|^2 + \frac{1}{2}gN|\Psi|^4\Big] \end{aligned}$$

where the Lagrangian density, is given by Eq.(20). Ψ is the trial wavefunction described above and has the following form (in scaled units),

$$\Psi(\bar{\mathbf{r}}, \bar{t}) = \frac{1}{\sqrt{N_c}} \sum_{j=1}^{N_c} A_j(\bar{t}) e^{f_j(\bar{\mathbf{r}},\bar{t}) + i\bar{\mathbf{k}}_j \cdot \bar{\mathbf{r}}} \tag{34}$$

with

$$\begin{aligned} f_j(\bar{\mathbf{r}},\bar{t}) &= -\frac{(\bar{x}-\bar{x}_j)^2}{2\bar{w}_{jx}^2} - \frac{(\bar{y}-\bar{y}_j)^2}{2\bar{w}_{jy}^2} - \frac{(\bar{z}-\bar{z}_j)^2}{2\bar{w}_{jz}^2} \\ &\quad + i\bar{\epsilon}_{jx}\bar{x} + i\bar{\epsilon}_{jy}\bar{y} + i\bar{\epsilon}_{jz}\bar{z} + i\bar{\beta}_{jx}\bar{x}^2 + i\bar{\beta}_{jy}\bar{y}^2 + i\bar{\beta}_{jz}\bar{z}^2 \\ &= \sum_{\eta=x,y,z}\left(-\frac{(\bar{\eta}-\bar{\eta}_j)^2}{2\bar{w}_{j\eta}^2} + i\bar{\epsilon}_{j\eta}\bar{\eta} + i\bar{\beta}_{j\eta}\bar{\eta}^2\right) \end{aligned} \tag{35}$$

where $\bar{\mathbf{r}} = (\bar{x},\bar{y},\bar{z})$ later we will denote the variational parameters as

$$\begin{aligned} \bar{\mathbf{x}} &\equiv (\bar{x}_1,\bar{y}_1,\bar{z}_1,\ldots,\bar{x}_{N_c},\bar{y}_{N_c},\bar{z}_{N_c}) \\ \bar{\mathbf{w}} &\equiv (\bar{w}_{1x},\bar{w}_{1y},\bar{w}_{1z},\ldots,\bar{w}_{xN_c},\bar{w}_{yN_c},\bar{w}_{zN_c}) \\ \bar{\boldsymbol{\epsilon}} &\equiv (\bar{\epsilon}_{1x},\bar{\epsilon}_{1y},\bar{\epsilon}_{1z},\ldots,\bar{\epsilon}_{xN_c},\bar{\epsilon}_{yN_c},\bar{\epsilon}_{zN_c}) \\ \bar{\boldsymbol{\beta}} &\equiv (\bar{\beta}_{1x},\bar{\beta}_{1y},\bar{\beta}_{1z},\ldots,\bar{\beta}_{xN_c},\bar{\beta}_{yN_c},\bar{\beta}_{zN_c}) \end{aligned}$$

The sets of variational parameters, $\{q(t)\}_j$ consist of the Cartesian coordinates of the j^{th} cloud center: $\bar{x}_j$, $\bar{y}_j$, and $\bar{z}_j$; the widths along the x, y, and z directions: $\bar{w}_{jx}$, $\bar{w}_{jy}$, and $\bar{w}_{jz}$; the linear phase coefficients along the x, y, and z directions: $\bar{\epsilon}_{jx}$, $\bar{\epsilon}_{jy}$, and $\bar{\epsilon}_{jz}$; and the quadratic phase coefficients along the x, y, and z directions: $\bar{\beta}_{jx}$, $\bar{\beta}_{jy}$, and $\bar{\beta}_{jz}$. These are all explicit functions of time. The j^{th} cloud also has its own normalization coefficient, A_j, which will be eliminated by fixing the number of atoms in each cloud.

4.1 Scaled Units

Before proceeding further, it is useful to define a set of scaled units appropriate to the system to simplify the calculations. This is done by first establishing a scaled *length unit*, L_0, and then an energy, E_0, and time, T_0, unit as follows

$$\begin{aligned} L_0 &= \text{length scale appropriate to system} \\ E_0 &\equiv \frac{\hbar^2}{2mL_0^2} \\ T_0 &\equiv \frac{\hbar}{E_0} = \frac{2mL_0^2}{\hbar} \end{aligned} \tag{36}$$

We can then introduce the scaled variables based on these units, which are generally denoted by barred quantities. To convert from SI units to scaled units we need to consider the dimensions of the quantity; for instance, the position x is measured in meters and has a dimension of length. To convert to scaled units express the SI quantity in terms of the product of the corresponding

scaled units quantity with the conversion factor, in this case L_0. Then the scaled spatial and temporal coordinates can be solved for as,

$$\begin{aligned} \bar{x} &\equiv \frac{x}{L_0} \\ \bar{y} &\equiv \frac{y}{L_0} \\ \bar{z} &\equiv \frac{z}{L_0} \\ \bar{t} &\equiv \frac{t}{T_0} \end{aligned} \tag{37}$$

We also introduce the scaled condensate wavefunction,

$$\bar{\Psi}(\bar{\mathbf{r}}, \bar{t}) = \Psi(\mathbf{r}, t) L_0^{3/2} \tag{38}$$

so then the RGPE in terms of scaled quantities is,

$$i\frac{\partial \bar{\Psi}}{\partial \bar{t}} = -\bar{\nabla}^2 \bar{\Psi} + \bar{V}_{\text{ext}}(\bar{\mathbf{r}}, \bar{t})\bar{\Psi} + \bar{g}N\left|\bar{\Psi}\right|^2 \bar{\Psi} + i\bar{\Omega}_z\left(\bar{x}\frac{\partial \bar{\Psi}}{\partial \bar{y}} - \bar{y}\frac{\partial \bar{\Psi}}{\partial \bar{x}}\right) \tag{39}$$

where $\bar{g} \equiv g/E_0 L_0^3$, and $\bar{V}(\bar{\mathbf{r}}, \bar{t}) = V(\mathbf{r}, t)/E_0$.

The associated scaled Lagrangian density is,

$$\bar{\mathcal{L}}[\bar{\Psi}^*, \bar{\Psi}^*_{\bar{\eta}}, \bar{\Psi}^*_{\bar{t}}, \bar{\eta}, \bar{t}] = \frac{i}{2}(\bar{\Psi}\bar{\Psi}^*_{\bar{t}} - \bar{\Psi}^*\bar{\Psi}_{\bar{t}}) + \left[\left|\bar{\boldsymbol{\nabla}}\bar{\Psi}\right|^2 + \bar{V}_{ext}(\bar{\mathbf{r}}, \bar{t})\left|\bar{\Psi}\right|^2 + \frac{1}{2}\bar{g}N\left|\bar{\Psi}\right|^4\right] \tag{40}$$

and the corresponding scaled Euler-Lagrange equation

$$\sum_{\bar{\eta}=\bar{x},\bar{y},\bar{z},\bar{t}} \frac{\partial}{\partial \bar{\eta}}\Big(\frac{\partial \bar{\mathcal{L}}}{\partial \bar{\Psi}^*_{\bar{\eta}}}\Big) - \frac{\partial \bar{\mathcal{L}}}{\partial \bar{\Psi}^*} = 0 \tag{41}$$

Finally, we can write down the scaled ordinary Lagrangian as follows,

$$\bar{L}(\bar{\mathbf{x}}, \bar{\mathbf{w}}, \bar{\boldsymbol{\epsilon}}, \bar{\boldsymbol{\beta}}) = \int_{-\infty}^{\infty} d^3\bar{r}\ \bar{\mathcal{L}}[\bar{\Psi}^*, \bar{\Psi}^*_{\bar{\eta}}, \bar{\Psi}^*_{\bar{t}}, \bar{\eta}, \bar{t}] \tag{42}$$

We can now write down the scaled ordinary Lagrangian as follows,

$$\begin{aligned} \bar{L}(\bar{\mathbf{x}}, \bar{\mathbf{w}}, \bar{\boldsymbol{\epsilon}}, \bar{\boldsymbol{\beta}}) &= \int_{-\infty}^{\infty} d^3\bar{r}\ \bar{\mathcal{L}}[\bar{\Psi}^*, \bar{\Psi}^*_{\bar{\eta}}, \bar{\Psi}^*_{\bar{t}}, \bar{\eta}, \bar{t}] \\ \bar{L} &= \int_{-\infty}^{\infty} d^3\bar{r}\ \left(\frac{i}{2}(\bar{\Psi}\bar{\Psi}^*_{\bar{t}} - \bar{\Psi}^*\bar{\Psi}_{\bar{t}}) + \left|\bar{\boldsymbol{\nabla}}\bar{\Psi}\right|^2 + \bar{V}_{ext}(\bar{\mathbf{r}}, \bar{t})\left|\bar{\Psi}\right|^2 + \frac{1}{2}\bar{g}N\left|\bar{\Psi}\right|^4\right) \end{aligned} \tag{43}$$

for visual clarity, we have split the terms up into separate integrals defined as follows,

$$\begin{aligned}
\bar{L} &= \bar{L}_1 + \bar{L}_2 + \bar{L}_3 + \bar{L}_4 \\
\bar{L}_1 &\equiv \int_{-\infty}^{\infty} d^3\bar{r} \frac{i}{2}(\bar{\Psi}\bar{\Psi}^*_{\bar{t}} - \bar{\Psi}^*\bar{\Psi}_{\bar{t}}) \\
\bar{L}_2 &\equiv \int_{-\infty}^{\infty} d^3\bar{r} \left|\bar{\boldsymbol{\nabla}}\bar{\Psi}\right|^2 \\
\bar{L}_3 &\equiv \int_{-\infty}^{\infty} d^3\bar{r} \bar{V}_{ext}(\bar{\mathbf{r}}, \bar{t}) \left|\bar{\Psi}\right|^2 \\
\bar{L}_4 &\equiv \int_{-\infty}^{\infty} d^3\bar{r} \frac{1}{2}\bar{g}N \left|\bar{\Psi}\right|^4
\end{aligned} \tag{44}$$

Any given equation of motion for a variational parameter associated to the j^{th} cloud, $q_j(\bar{t})$ is given by the standard Euler-Lagrange equation as follows:

$$\frac{\partial}{\partial\bar{t}}\left(\frac{\partial\bar{L}}{\partial\dot{q}_j}\right) - \frac{\partial\bar{L}}{\partial q_j} = 0; \qquad j = 1, 2, \ldots, N_c \tag{45}$$

The procedure with these tools is to calculate the total ordinary Lagrangian by determining the above L's using the trial wavefunction, which is the sum of N_c 3-D Gaussian clouds. Then using the standard Euler-Lagrange equations derive equations of motion for each variational parameter; fortunately, as we'll see, these form a closed set of equations so that only the centers and widths, along with their time derivatives, need to be solved for. Any other variational parameter can be written in terms of them. For a detailed treatment of the 1-D N_c cloud model see Ref. [48].

4.2 Constraints on the trial wavefunction

Here we make several assumptions about the physical system which have material effects on the values of the variational parameters. These are as follows:

1. We assume that each of the N_c clouds are moving at sufficiently different velocities such that any integral of a quantity containing a factor like $e^{i\left(\bar{k}_{j\eta} - \bar{k}_{j'\eta}\right)\bar{\eta}}$ where $j \neq j'$ can be neglected. If the clouds move with sufficiently different velocities, these factors will be rapidly oscillating and their integrals can be neglected.

2. The $A_j(\bar{t})$ are real for all j. This derives from the assumption that the system is a single condensate and has an overall constant phase.

3. The number of atoms in each cloud is fixed. Clouds do not exchange atoms. This plus the normalization condition, fixes a relationship between A_j and the widths $\bar{w}_{j\eta}$ where $\eta = x, y, z$.

We can use these assumptions plus the normalization condition on the trial wave function to derive conditions that constrain the values of the A_j. Furthermore, our assumption that the number of atoms in each cloud is fixed adds the further restriction that each cloud is individually normalized. This gives finally,

$$A_j^2(\bar{t})\pi^{3/2}\bar{w}_{jx}(\bar{t})\bar{w}_{jy}(\bar{t})\bar{w}_{jz}(\bar{t}) = 1; \qquad j = 1, \ldots, N_c. \tag{46}$$

4.3 Equations of Motion for the Rotating Frame

The equations of motion for the are a set of second–order ordinary differential equation for the cloud centers, $\bar{\eta_j}$, and widths, $\bar{w}_{j\eta}$, as well as expressions for the $\bar{\beta}_{j\eta}$ and the $\bar{\epsilon}_{j\eta}$ in terms of the centers, widths and their first derivatives. After transforming to the rotating frame (about the z-axis) we have:

$$\ddot{\bar{x}}_j = 2\bar{\Omega}_z\dot{\bar{y}}_j + \bar{\Omega}_z^2\bar{x}_j - \frac{\partial\bar{U}^{(3D)}}{\partial\bar{x}_j}, \tag{47a}$$

$$\ddot{\bar{y}}_j = -2\bar{\Omega}_z\dot{\bar{x}}_j + \bar{\Omega}_z^2\bar{y}_j - \frac{\partial\bar{U}^{(3D)}}{\partial\bar{y}_j}, \tag{47b}$$

$$\ddot{\bar{z}}_j = -\frac{\partial\bar{U}^{(3D)}}{\partial\bar{z}_j}, \tag{47c}$$

$$\ddot{\bar{w}}_{j\eta} = \frac{4}{\bar{w}_{j\eta}^3} - 2\frac{\partial\bar{U}^{(3D)}}{\partial\bar{w}_{j\eta}}, \tag{47d}$$

$$\bar{\beta}_{j\eta} = \frac{\dot{\bar{w}}_{j\eta}}{4\bar{w}_{j\eta}}, \tag{47e}$$

$$\bar{\epsilon}_{jx} = \tfrac{1}{2}(\dot{\bar{x}}_j - \bar{\Omega}_z\bar{y}_j) - 2\bar{\beta}_{jx}\bar{x}_j, \tag{47f}$$

$$\bar{\epsilon}_{jy} = \tfrac{1}{2}(\dot{\bar{y}}_j + \bar{\Omega}_z\bar{x}_j) - 2\bar{\beta}_{jy}\bar{y}_j, \tag{47g}$$

$$\bar{\epsilon}_{jz} = \tfrac{1}{2}\dot{\bar{z}}_j - 2\bar{\beta}_{jx}\bar{x}_j, \tag{47h}$$

$$\eta = x, y, z \qquad j = 1, \ldots, N_c$$

The equations for the cloud centers and cloud widths (Eqs. (47a), (47b), (47c), and (47d)) form a closed set that contain only the $\bar{\eta}_j$, $\dot{\bar{\eta}}_j$, $\bar{w}_{j\eta}$, and $\dot{\bar{w}}_{j\eta}$. Once these quantities are obtained, all of the other variational parameters can be calculated.

The factor $\bar{U}^{(3D)}(\bar{\mathbf{x}}, \bar{\mathbf{w}})$ is the "variational potential"

$$\begin{aligned}\bar{U}^{(3D)}(\bar{\mathbf{x}}, \bar{\mathbf{w}}) &\equiv 2N_c\bar{L}_3(\bar{\mathbf{x}}, \bar{\mathbf{w}}) + 2N_c\bar{L}_4(\bar{\mathbf{x}}, \bar{\mathbf{w}}) \\ &\equiv \bar{U}_{\text{ext}}^{(3D)}(\bar{\mathbf{x}}, \bar{\mathbf{w}}) + \bar{U}_{\text{int}}^{(3D)}(\bar{\mathbf{x}}, \bar{\mathbf{w}}).\end{aligned} \tag{48}$$

The external and interaction variational potentials are the expectation values of the actual

external potential and the condensate density over the trial wave function respectively. We've grouped two different methods of interactions for consideration in the model, self and cloud-cloud. Self accounts for the interactions between atoms in a particular condensate which causes the clouds to expand and contract; and cloud-cloud for the interactions between atoms in different clouds which occur only when two or more clouds overlap.

The expression for $\bar{U}_{\text{ext}}^{(3D)}(\bar{\mathbf{x}}, \bar{\mathbf{w}})$ is

$$\bar{U}_{\text{ext}}^{(3D)}(\bar{\mathbf{x}}, \bar{\mathbf{w}}) \equiv 2N_c \int_{-\infty}^{\infty} d^3\bar{r}\, \bar{\Psi}^*(\bar{\mathbf{r}}, \bar{t}) \bar{V}_{\text{ext}}(\bar{\mathbf{r}}, \bar{t}) \bar{\Psi}(\bar{\mathbf{r}}, \bar{t}) \tag{49a}$$

$$= \sum_{j=1}^{N_c} \left(\frac{2}{\pi^{3/2} \bar{w}_{jx} \bar{w}_{jy} \bar{w}_{jz}} \right) \tag{49b}$$

$$\times \int_{-\infty}^{\infty} d^3\bar{r}\, \exp\left\{ - \sum_{\eta=x,y,z} \frac{(\bar{\eta} - \bar{\eta}_j)^2}{\bar{w}_{j\eta}^2} \right\} \bar{V}_{\text{ext}}(\bar{\mathbf{r}}, \bar{t})$$

where $\bar{V}_{\text{ext}}(\bar{\mathbf{r}}, \bar{t})$ is the actual external potential, in scaled units.

The expression for $\bar{U}_{\text{int}}(\bar{\mathbf{x}}, \bar{\mathbf{w}})$ is given by

$$\bar{U}_{\text{int}}(\bar{\mathbf{x}}, \bar{\mathbf{w}}) \equiv N_c \bar{g} N \int_{-\infty}^{\infty} d\bar{x} \int_{-\infty}^{\infty} d\bar{y} \int_{-\infty}^{\infty} d\bar{z}\, \left(\Psi^*(\bar{\mathbf{r}}, \bar{t})\right)^2 \left(\Psi(\bar{\mathbf{r}}, \bar{t})\right)^2 \tag{50}$$

which, given a trial wavefunction, will always be the same for any number of clouds.

The equations of motion (EOM) for the cloud centers and widths are valid for any external potential. It's worth noting that this variational potential will only be a function of the center and width parameters of all of the Gaussians. Also we can consider the derivatives of the "variational potential" that appear in the EOM as consisting of two force terms: one is the familiar force associated to the spatial and width derivatives of the external potential, $\frac{\partial \bar{U}_{\text{ext}}}{\partial \eta}$, $\frac{\partial \bar{U}_{\text{ext}}}{\partial \bar{w}_{j\eta}}$, and the other is the spatial and width derivatives of the internal potential, $\frac{\partial \bar{U}_{\text{int}}}{\partial \eta}$, $\frac{\partial \bar{U}_{\text{int}}}{\partial \bar{w}_{j\eta}}$. These correspond to a force due to interactions, cloud-cloud and self respectively. This is a useful recognition as it allows one to probe the effect of interactions with the model easily as we can rewrite the EOM

(for the spatial and width parameters) as follows,

$$\ddot{\bar{x}}_j = 2\bar{\Omega}_z\dot{\bar{y}}_j + \bar{\Omega}_z^2\bar{x}_j - \frac{\partial\bar{U}_{ext}^{(3D)}}{\partial\bar{x}_j} - F_{jx}(\bar{\mathbf{x}},\bar{\mathbf{w}}), \tag{51a}$$

$$\ddot{\bar{y}}_j = -2\bar{\Omega}_z\dot{\bar{x}}_j + \bar{\Omega}_z^2\bar{y}_j - \frac{\partial\bar{U}_{ext}^{(3D)}}{\partial\bar{y}_j} - F_{jy}(\bar{\mathbf{x}},\bar{\mathbf{w}}),$$

$$\ddot{\bar{z}}_j = \frac{\partial\bar{U}_{ext}^{(3D)}}{\partial\bar{z}_j} - F_{jz}(\bar{\mathbf{x}},\bar{\mathbf{w}}),$$

$$\ddot{\bar{w}}_{j\eta} = \frac{4}{\bar{w}_{j\eta}^3} - 2\frac{\partial\bar{U}_{ext}^{(3D)}}{\partial\bar{w}_{j\eta}} + \frac{2\bar{g}N}{(2\pi)^{3/2}N_c}\Big(\frac{1}{\bar{w}_{jx}\bar{w}_{jy}\bar{w}_{jz}\bar{w}_{j\eta}}\Big) - W_{j\eta}(\bar{\mathbf{x}},\bar{\mathbf{w}}),$$

$$\eta = x,y,z \qquad j = 1,\ldots,N_c$$

where $F_{j\eta}(\bar{\mathbf{x}},\bar{\mathbf{w}})$, the third term in $\ddot{\bar{w}}_{j\eta}$, and $W_{j\eta}(\bar{\mathbf{x}},\bar{\mathbf{w}})$ are terms arising from the spatial and width gradients of $\bar{U}_{int}^{(3D)}(\bar{\mathbf{x}},\bar{\mathbf{w}})$. $F_{j\eta}(\bar{\mathbf{x}},\bar{\mathbf{w}})$ accounts for interaction forces exerted on the cloud-center of the j^{th} cloud due to cloud-cloud interactions with one or more other clouds. The third term in $\ddot{\bar{w}}_{j\eta}$ accounts for the effects of self interactions within the j^{th} cloud which causes the cloud to expand and contract. $W_{j\eta}(\bar{\mathbf{x}},\bar{\mathbf{w}})$ accounts for the evolution of the width of the j^{th} cloud due to cloud-cloud interactions with one or more other clouds. This model is capable of simulating extreme atom interferometry processes such as multiple high–momentum clouds, large volumes, and long interrogation times in a few minutes on a commodity desktop computer. The standard methodology of solving the GPE would require an impractical amount of run time and storage to provide accurate solutions at the same scale.

4.4 Power Law Potential

This model can be implemented for any arbitrary external potential. In this section we outline the usage of an arbitrary 3-D power law potential in order to account for the anharmonic potential in the experiment carried out at UVa. This potential is of the following form,

$$\bar{V}_{\text{ext}}(\bar{\mathbf{r}}) \equiv \sum_{k=1}^{N_{\text{terms}}} C_{p_x(k),p_y(k),p_z(k)}\bar{x}^{p_x(k)}\bar{y}^{p_y(k)}\bar{z}^{p_z(k)}. \tag{52}$$

If we include all triples, (p_x,p_y,p_z), of powers such that

$$p_x+p_y+p_z \le N_{\max} \quad \text{then} \quad N_{\text{terms}} = \frac{1}{6}N_{\max}\left(N_{\max}^2+6N_{\max}+11\right) \tag{53}$$

excluding the term where all powers are zero. In the case of the UVa experiment we have $N_{\max}=4$ and then the number of terms is $N_{\text{terms}}=34$. Placing this potential into Eq.(49c) we

arrive at:

$$
\begin{aligned}
\bar{U}_{\rm ext}(\bar{\mathbf{x}},\bar{\mathbf{w}}) &= \sum_{j=1}^{N_c}\left(\frac{2}{\pi^{3/2}\bar{w}_{jx}\bar{w}_{jy}\bar{w}_{jz}}\right) \\
&\times \int d^3\bar{r}\,\exp\left\{-\sum_{\eta=x,y,z}\frac{(\bar{\eta}-\bar{\eta}_j)^2}{\bar{w}_{j\eta}^2}\right\}\bar{V}_{\rm ext}(\bar{\mathbf{r}},\bar{t}) \\
&= \sum_{k=1}^{N_{\rm terms}} C_{p_x(k),p_y(k),p_z(k)} \sum_{j=1}^{N_c}\left(\frac{2}{\pi^{3/2}\bar{w}_{jx}\bar{w}_{jy}\bar{w}_{jz}}\right) \\
&\times \int d^3\bar{r}\, e^{-(\bar{x}-\bar{x}_j)^2/\bar{w}_{jx}^2} e^{-(\bar{y}-\bar{y}_j)^2/\bar{w}_{jy}^2} e^{-(\bar{z}-\bar{z}_j)^2/\bar{w}_{jz}^2} \bar{x}^{p_x(k)}\bar{y}^{p_y(k)}\bar{z}^{p_z(k)} \\
&= \sum_{k=1}^{N_{\rm terms}} C_{p_x(k),p_y(k),p_z(k)} \sum_{j=1}^{N_c}\left(\frac{2}{\pi^{3/2}\bar{w}_{jx}\bar{w}_{jy}\bar{w}_{jz}}\right) \\
&\times \int_{-\infty}^{+\infty} d\bar{x}\,\bar{x}^{p_x(k)} e^{-(\bar{x}-\bar{x}_j)^2/\bar{w}_{jx}^2} \int_{-\infty}^{+\infty} d\bar{y}\,\bar{y}^{p_y(k)} e^{-(\bar{y}-\bar{y}_j)^2/\bar{w}_{jy}^2} \\
&\times \int_{-\infty}^{+\infty} d\bar{z}\,\bar{z}^{p_z(k)} e^{-(\bar{z}-\bar{z}_j)^2/\bar{w}_{jz}^2} \\
&= \sum_{k=1}^{N_{\rm terms}} C_{p_x(k),p_y(k),p_z(k)} \sum_{j=1}^{N_c}\left(\frac{2}{\pi^{3/2}\bar{w}_{jx}\bar{w}_{jy}\bar{w}_{jz}}\right) J_{p_x(k)}(\bar{x}_j,\bar{w}_{jx}) \\
&\times J_{p_y(k)}(\bar{y}_j,\bar{w}_{jy}) J_{p_z(k)}(\bar{z}_j,\bar{w}_{jz})
\end{aligned}
\tag{54}
$$

where we have defined

$$
J_k(\bar{\eta}_0,\bar{w}_{0\eta}) \equiv \int_{-\infty}^{\infty} \bar{\eta}^k e^{-(\bar{\eta}-\bar{\eta}_0)^2/\bar{w}_{0\eta}^2}\, d\bar{\eta}, \quad k=0,1,2,\ldots \tag{55}
$$

we can evaluate this class of integrals by changing the variable of integration:

$$
x \equiv \frac{\eta-\bar{\eta}_0}{\bar{w}_{0\eta}}, \quad \eta = \bar{\eta}_0 + \bar{w}_{0\eta}x, \quad d\eta = \bar{w}_{0\eta}dx. \tag{56}
$$

Expressed in terms of this new integration variable, the integral now has the form

$$
J_k(\bar{\eta}_0,\bar{w}_{0\eta}) = \int_{-\infty}^{\infty} \left(\bar{\eta}_0 + \bar{w}_{0\eta}x\right)^k e^{-x^2}\, \bar{w}_{0\eta}dx. \tag{57}
$$

We now use the binomial theorem to express the factor $(\bar{\eta}_0 + \bar{w}_{0\eta}x)^k$ as a series of powers of x:

$$
\left(\bar{\eta}_0 + \bar{w}_{0\eta}x\right)^k = \sum_{s=0}^{k}\binom{k}{s}\bar{\eta}_0^{k-s}\left(\bar{w}_{0\eta}x\right)^s. \tag{58}
$$

Inserting this into the integral in Eq. (57) gives

$$
J_k(\bar{\eta}_0,\bar{w}_{0\eta}) = \bar{w}_{0\eta}\sum_{s=0}^{k}\binom{k}{s}\bar{\eta}_0^{k-s}\bar{w}_{0\eta}^s \int_{-\infty}^{\infty} x^s e^{-x^2}\, dx. \tag{59}
$$

The integral now appearing in the sum above is well–known (after all, integration is the art of transforming the integral until you can look it up!). We have

$$\int_{-\infty}^{\infty} x^s e^{-x^2}\, dx = \left\{ \begin{array}{ll} 0 & s = \text{ odd integer} \\ \left(\frac{s!}{(s/2)!}\right) \frac{\pi^{1/2}}{2^s} & s = \text{ even integer} \end{array} \right\} \tag{60}$$

Using this result we can write a final expression for the integrals:

$$\begin{aligned} J_k\left(\bar{\eta}_0, \bar{w}_{0\eta}\right) &= \left(\bar{w}_{0\eta}\pi^{1/2}\right) \sum_{m=0}^{[k/2]} \binom{k}{2m} \bar{\eta}_0^{k-2m} \left(\frac{\bar{w}_{0\eta}}{2}\right)^{2m} \frac{(2m)!}{m!} \\ &= \left(\bar{w}_{0\eta}\pi^{1/2}\right) \sum_{m=0}^{[k/2]} \left(\frac{k!}{m!(k-2m)!}\right) \bar{\eta}_0^{k-2m} (\tfrac{1}{2}\bar{w}_{0\eta})^{2m} \\ &\equiv \left(\bar{w}_{0\eta}\pi^{1/2}\right) \bar{J}_k\left(\bar{\eta}_0, \bar{w}_{0\eta}\right). \end{aligned}$$

Where the upper limit of the sum, $[k/2]$, is the greatest integer less than or equal to $k/2$. Also $[m]$ is the greatest integer less than or equal to n and we have introduced the function

$$\bar{J}_k\left(\bar{\eta}, \bar{w}_\eta\right) = \sum_{m=0}^{[k/2]} \left(\frac{k!}{m!(k-2m)!}\right) \bar{\eta}^{k-2m} (\tfrac{1}{2}\bar{w}_\eta)^{2m}. \tag{61}$$

This newly defined function, $\bar{J}_k(\bar{\eta}, \bar{w_\eta})$, allows us to write the potential in a more compact form by removing the . The potential becomes

$$\begin{aligned} \bar{U}_{\text{ext}}\left(\bar{\mathbf{x}}, \bar{\mathbf{w}}\right) &= 2 \sum_{j_1=1}^{N_c} \sum_{k=1}^{N_{\text{terms}}} C_{p_x(k),p_y(k),p_z(k)} \bar{J}_{p_x(k)}(\bar{x}_{j_1}, \bar{w}_{j_1 x}) \\ &\times \bar{J}_{p_y(k)}(\bar{y}_{j_1}, \bar{w}_{j_1 y}) \bar{J}_{p_z(k)}(\bar{z}_{j_1}, \bar{w}_{j_1 z}) \end{aligned} \tag{62}$$

and we can rewrite the definition of $\bar{J}_k(\bar{\eta}, \bar{w}_\eta)$ as

$$\bar{J}_k(\bar{\eta}, \bar{w}_\eta) = \left\{ \begin{array}{ll} \sum_{m=0}^{k/2} \left(\frac{k!}{m!(k-2m)!}\right) \bar{\eta}^{k-2m} (\frac{1}{2}\bar{w}_\eta)^{2m} & \text{k = even integer} \\ \sum_{m=0}^{(k-1)/2} \left(\frac{k!}{m!(k-2m)!}\right) \bar{\eta}^{k-2m} (\frac{1}{2}\bar{w}_\eta)^{2m} & \text{k = odd integer} \end{array} \right\} \tag{63}$$

To derive the equations of motion (Eqs. (47a)–(47d)) for this power law external potential we need to consider the spatial and width derivatives of external variational potential calculated in Eq. (55), along with those of the internal variational potential. These are given below. We reiterate here that the corresponding equations of motion apply to any system of N_c condensate

clouds subject to the power–law potential defined above.

$$
\begin{aligned}
\frac{\partial \bar{U}_{\rm ext}}{\partial \bar{x}_j} &= 2\sum_{k=1}^{N_{\rm terms}} C_{p_x(k),p_y(k),p_z(k)} \left(\frac{\partial \bar{J}_{p_x(k)}}{\partial \bar{x}_j}\right) \bar{J}_{p_y(k)}(\bar{y}_j,\bar{w}_{jy})\bar{J}_{p_z(k)}(\bar{z}_j,\bar{w}_{jz}) \\
\frac{\partial \bar{U}_{\rm ext}}{\partial \bar{y}_j} &= 2\sum_{k=1}^{N_{\rm terms}} C_{p_x(k),p_y(k),p_z(k)} \bar{J}_{p_x(k)}(\bar{x}_j,\bar{w}_{jx}) \left(\frac{\partial \bar{J}_{p_y(k)}}{\partial \bar{y}_j}\right) \bar{J}_{p_z(k)}(\bar{z}_j,\bar{w}_{jz}) \\
\frac{\partial \bar{U}_{\rm ext}}{\partial \bar{z}_j} &= 2\sum_{k=1}^{N_{\rm terms}} C_{p_x(k),p_y(k),p_z(k)} \bar{J}_{p_x(k)}(\bar{x}_j,\bar{w}_{jx})\bar{J}_{p_y(k)}(\bar{y}_j,\bar{w}_{jy}) \left(\frac{\partial \bar{J}_{p_z(k)}}{\partial \bar{z}_j}\right) \\
\frac{\partial \bar{U}_{\rm ext}}{\partial \bar{w}_{jx}} &= 2\sum_{k=1}^{N_{\rm terms}} C_{p_x(k),p_y(k),p_z(k)} \left(\frac{\partial \bar{J}_{p_x(k)}}{\partial \bar{w}_{jx}}\right) \bar{J}_{p_y(k)}(\bar{y}_j,\bar{w}_{jy})\bar{J}_{p_z(k)}(\bar{z}_j,\bar{w}_{jz}) \\
\frac{\partial \bar{U}_{\rm ext}}{\partial \bar{w}_{jy}} &= 2\sum_{k=1}^{N_{\rm terms}} C_{p_x(k),p_y(k),p_z(k)} \bar{J}_{p_x(k)}(\bar{x}_j,\bar{w}_{jx}) \left(\frac{\partial \bar{J}_{p_y(k)}}{\partial \bar{w}_{jy}}\right) \bar{J}_{p_z(k)}(\bar{z}_j,\bar{w}_{jz}) \\
\frac{\partial \bar{U}_{\rm ext}}{\partial \bar{w}_{jz}} &= 2\sum_{k=1}^{N_{\rm terms}} C_{p_x(k),p_y(k),p_z(k)} \bar{J}_{p_x(k)}(\bar{x}_j,\bar{w}_{jx})\bar{J}_{p_y(k)}(\bar{y}_j,\bar{w}_{jy}) \left(\frac{\partial \bar{J}_{p_z(k)}}{\partial \bar{w}_{jz}}\right).
\end{aligned}
$$

and the derivatives can be expressed as follows.

$$
\frac{\partial \bar{J}_k}{\partial \bar{\eta}} = \left\{ \begin{array}{ll} \sum_{m=0}^{k/2} \left(\frac{k!}{m!(k-2m-1)!}\right) \bar{\eta}^{k-2m-1} (\frac{1}{2}\bar{w}_\eta)^{2m} & \text{k = even integer} \\ \sum_{m=0}^{(k-1)/2} \left(\frac{k!}{m!(k-2m-1)!}\right) \bar{\eta}^{k-2m-1} (\frac{1}{2}\bar{w}_\eta)^{2m} & \text{k = odd integer} \end{array} \right\} \tag{64}
$$

and

$$
\frac{\partial \bar{J}_k}{\partial \bar{w}_\eta} = \left\{ \begin{array}{ll} \sum_{m=1}^{k/2} \left(\frac{k!}{(m-1)!(k-2m)!}\right) \bar{\eta}^{k-2m} (\frac{1}{2}\bar{w}_\eta)^{2m-1} & \text{k = even integer} \\ \sum_{m=1}^{(k-1)/2} \left(\frac{k!}{(m-1)!(k-2m)!}\right) \bar{\eta}^{k-2m} (\frac{1}{2}\bar{w}_\eta)^{2m-1} & \text{k = odd integer} \end{array} \right\} \tag{65}
$$

The internal variational potential given by Eq. (50) is the same for any number of clouds and so it can be calculated once and for all. The expressions for the derivatives that appear in the equations of motion are given by

$$
\begin{aligned}
F_{j\eta}(\bar{\mathbf{x}},\bar{\mathbf{w}}) \equiv \frac{\partial \bar{U}_{\rm int}}{\partial \bar{\eta}_j} = \left(\frac{8\bar{g}N}{(\pi)^{3/2}N_c}\right) \sum_{\substack{j'=1 \\ j'\neq j}}^{N_c} \prod_{\eta'=x,y,z} \left(\frac{\exp\left\{-\frac{(\bar{\eta'}_{j'}-\bar{\eta'}_j)^2}{\bar{w}^2_{j'\eta'}+\bar{w}^2_{j\eta'}}\right\}}{\left(\bar{w}^2_{j'\eta'}+\bar{w}^2_{j\eta'}\right)^{1/2}} \right) \\
\times \quad \left(\frac{(\bar{\eta}_{j'}-\bar{\eta}_j)}{\bar{w}^2_{j'\eta}+\bar{w}^2_{j\eta}}\right)
\end{aligned} \tag{66}
$$

and

$$
2\frac{\partial \bar{U}_{\rm int}}{\partial \bar{w}_{j\eta}} \equiv 2\frac{(\bar{g}N)}{(2\pi)^{3/2}N_c} \left(\frac{-1}{\bar{w}_{jx}\bar{w}_{jy}\bar{w}_{jz}\bar{w}_{j\eta}}\right) + W_{j\eta}(\bar{\mathbf{x}},\bar{\mathbf{w}}) \tag{67}
$$

where the first term accounts for the self interactions and the second accounts for cloud-cloud

interactions with,

$$W_{j\eta}(\bar{\mathbf{x}},\bar{\mathbf{w}}) \equiv 2\frac{(4\bar{g}N)}{(\pi)^{3/2}N_c}\sum_{\substack{j_1=1\\ j_1\neq j}}^{N_c}\prod_{\eta'=x,y,z}\left(\frac{\exp\left\{-\frac{\left(\bar{\eta'}_{j_1}-\bar{\eta'}_j\right)^2}{\bar{w}^2_{j_1\eta'}+\bar{w}^2_{j\eta'}}\right\}}{\left(\bar{w}^2_{j_1\eta'}+\bar{w}^2_{j\eta'}\right)^{1/2}}\right) \times \left(\frac{\bar{w}_{j\eta}\left(2\left(\bar{\eta}_{j_1}-\bar{\eta}_j\right)^2-\left(\bar{w}^2_{j_1\eta}+\bar{w}^2_{j\eta}\right)\right)}{\left(\bar{w}^2_{j_1\eta}+\bar{w}^2_{j\eta}\right)^2}\right). \tag{68}$$

The phase parameters can then be written in terms of the center coordinates and widths and their derivatives. These are given by

$$\bar{\beta}_{j\eta} = \frac{\dot{\bar{w}}_{j\eta}}{4\bar{w}_{j\eta}}, \tag{69a}$$

$$\bar{\epsilon}_{jx} = \tfrac{1}{2}(\dot{\bar{x}}_j - \bar{\Omega}_z\bar{y}_j) - 2\bar{\beta}_{jx}\bar{x}_j - \bar{k}_{jx}, \tag{69b}$$

$$\bar{\epsilon}_{jy} = \tfrac{1}{2}(\dot{\bar{y}}_j + \bar{\Omega}_z\bar{x}_j) - 2\bar{\beta}_{jy}\bar{y}_j - \bar{k}_{jy}, \tag{69c}$$

$$\bar{\epsilon}_{jz} = \tfrac{1}{2}\dot{\bar{z}}_j - 2\bar{\beta}_{jz}\bar{z}_j - \bar{k}_{jz}, \tag{69d}$$

$$\eta = x,y,z \qquad j = 1,\ldots,N_c$$

4.4.1 UVa Anharmonic Potential

We can derive the equations of motion for the particular case of the anharmonic potential present in the UVa experiment given in Eq. (33) and shown below for convenience,

$$V(\mathbf{r}) = m\omega_0^2[\frac{1}{2}\rho^2 + \frac{\lambda^2}{2}z^2 + \frac{1}{3}az^3 + \frac{1}{2}b\rho^2 z + \frac{1}{4}c\rho^4 + \frac{1}{4}fz^4 + \frac{1}{2}h\rho^2 z^2]$$

where the horizontal frequency ω_0 is,

$$\omega_0 = (\frac{7}{64}\frac{\mu}{m}\frac{B_1^2}{B_0})^{1/2}$$

also the coefficients are,

$$\lambda^2 = \frac{8}{7} \quad a = \frac{6}{7}\kappa \quad b = \frac{9}{14}\kappa \quad c = -\frac{237}{3584}\kappa^2 \quad f = \frac{17}{28}\kappa^2 \quad h = \frac{93}{224}\kappa^2$$

This potential can be written in the form of the general power–law potential defined in Eq. (52)

in scaled units as follows:

$$\begin{aligned}\bar{V}_{\rm ext}(\bar{\mathbf{r}}) &= \bar{C}_{200}\bar{x}^2\bar{y}^0\bar{z}^0 + \bar{C}_{020}\bar{x}^0\bar{y}^2\bar{z}^0 + \bar{C}_{002}\bar{x}^0\bar{y}^0\bar{z}^2 \\ &+ \bar{C}_{201}\bar{x}^2\bar{y}^0\bar{z}^1 + \bar{C}_{021}\bar{x}^0\bar{y}^2\bar{z}^1 + \bar{C}_{003}\bar{x}^0\bar{y}^0\bar{z}^3 \\ &+ \bar{C}_{400}\bar{x}^0\bar{y}^0\bar{z}^4 + \bar{C}_{220}\bar{x}^2\bar{y}^2\bar{z}^0 + \bar{C}_{040}\bar{x}^0\bar{y}^4\bar{z}^0 \\ &+ \bar{C}_{202}\bar{x}^2\bar{y}^0\bar{z}^2 + \bar{C}_{022}\bar{x}^0\bar{y}^2\bar{z}^2 + \bar{C}_{004}\bar{x}^0\bar{y}^0\bar{z}^4. \end{aligned} \tag{70}$$

The coefficients given in the UVa potential, in SI units, can be converted to scaled coefficients by dividing both sides of Eq. (33) by E_0 and noting that each term then has the common factor $\frac{1}{2}\omega_0^2/E_0 = \frac{1}{4}\bar{\omega}_0^2/L_0^2$ where $\omega_0 = \bar{\omega}_0/T_0^2$. The scaled coefficients can then be written as

$$\bar{C}_{200} = \bar{C}_{020} = \bar{C}_{002}/\lambda^2 = \tfrac{1}{4}\bar{\omega}_0^2, \quad \bar{C}_{201} = \bar{C}_{021} = \tfrac{1}{4}\bar{\omega}_0^2\bar{b}, \quad \bar{C}_{003} = \tfrac{1}{6}\bar{\omega}_0^2\bar{a}$$

$$\bar{C}_{400} = \bar{C}_{040} = \bar{C}_{220}/2 = \tfrac{1}{8}\bar{\omega}_0^2\bar{c}, \quad \bar{C}_{202} = \bar{C}_{022} = \tfrac{1}{4}\bar{\omega}_0^2\bar{h}, \quad \bar{C}_{004} = \tfrac{1}{8}\bar{\omega}_0^2\bar{f}$$

where $\bar{a} = a/L_0$, $\bar{b} = b/L_0$, $\bar{c} = c/L_0^2$, $\bar{f} = f/L_0^2$, and $\bar{h} = h/L_0^2$.

We can find the external variational potential, $\bar{U}_{\rm ext}^{(3D)}$, corresponding to the scaled UVa anharmonic potential given above in Eq. (71) by using Eq. (63) for the general power–law potential. Each term, $\bar{C}_{\alpha\beta\gamma}\bar{x}^\alpha\bar{y}^\beta\bar{z}^\gamma$, in $\bar{V}_{\rm ext}$ has a corresponding term in $\bar{U}_{\rm ext}^{(3D)}$, namely

$$\bar{C}_{\alpha\beta\gamma}\bar{J}_\alpha(\bar{x}_j,\bar{w}_{jx})\bar{J}_\beta(\bar{y}_j,\bar{w}_{jy})\bar{J}_\gamma(\bar{z}_j,\bar{w}_{jz}).$$

Since the maximum power is 4 we only need $\bar{J}_n(\bar{\eta},\bar{w}_\eta)$ for powers $n = 1, 2, 3, 4$. These are $\bar{J}_0 = 1$, $\bar{J}_1 = \bar{\eta}$, $\bar{J}_2 = \bar{\eta}^2 + \frac{1}{2}\bar{w}_\eta^2$, $\bar{J}_3 = \bar{\eta}^3 + \frac{3}{2}\bar{\eta}\bar{w}_\eta^2$, and $\bar{J}_4 = \bar{\eta}^4 + 3\bar{\eta}^2\bar{w}_\eta^2 + \frac{3}{4}\bar{w}_\eta^4$. This process yields the specific form of $\bar{U}_{\rm ext}^{(3D)}$ for the UVa anharmonic potential. The result is

$$\begin{aligned}\bar{U}_{\rm ext}^{(3D)}(\bar{\mathbf{x}},\bar{\mathbf{w}}) &= 2\sum_{j=1}^{N_c}\Big(\bar{C}_{200}(\bar{x}_j^2 + \tfrac{1}{2}\bar{w}_{jx}^2) + \bar{C}_{020}(\bar{y}_j^2 + \tfrac{1}{2}\bar{w}_{jy}^2) + \bar{C}_{002}(\bar{z}_j^2 + \tfrac{1}{2}\bar{w}_{jz}^2) \\ &+ \bar{C}_{201}(\bar{x}_j^2 + \tfrac{1}{2}\bar{w}_{jx}^2)\bar{z}_j + \bar{C}_{021}(\bar{y}_j^2 + \tfrac{1}{2}\bar{w}_{jy}^2)\bar{z}_j + \bar{C}_{003}(\bar{z}_j^3 + \tfrac{3}{2}\bar{z}_j\bar{w}_{jz}^2) \\ &+ \bar{C}_{400}(\bar{x}_j^4 + 3\bar{x}_j^2\bar{w}_{jx}^2 + \tfrac{3}{4}\bar{w}_{jx}^4) + \bar{C}_{220}(\bar{x}_j^2 + \tfrac{1}{2}\bar{w}_{jx}^2)(\bar{y}_j^2 + \tfrac{1}{2}\bar{w}_{jy}^2) \\ &+ \bar{C}_{040}(\bar{y}_j^4 + 3\bar{y}_j^2\bar{w}_{jy}^2 + \tfrac{3}{4}\bar{w}_{jy}^4) + \bar{C}_{202}(\bar{x}_j^2 + \tfrac{1}{2}\bar{w}_{jx}^2)(\bar{z}_j^2 + \tfrac{1}{2}\bar{w}_{jz}^2) \\ &+ \bar{C}_{022}(\bar{y}_j^2 + \tfrac{1}{2}\bar{w}_{jy}^2)(\bar{z}_j^2 + \tfrac{1}{2}\bar{w}_{jz}^2) \\ &+ \bar{C}_{004}(\bar{z}_j^4 + 3\bar{z}_j^2\bar{w}_{jz}^2 + \tfrac{3}{4}\bar{w}_{jz}^4)\Big). \end{aligned} \tag{71}$$

This potential can be used to write down the equations of motion for the specific case of the anharmonic potential. We first need to consider the spatial and width derivatives of $\bar{U}_{ext}^{(3D)}$,

after these are determined we can then immediately write down the equations of motion. For example, consider

$$\begin{aligned}
\frac{\partial \bar{U}_{\rm ext}}{\partial \bar{x}_j} &= 2\sum_{k=1}^{N_{\rm terms}} \bar{C}_{p_x(k),p_y(k),p_z(k)} \left(\frac{\partial \bar{J}_{p_x(k)}}{\partial \bar{x}_j}\right) \bar{J}_{p_y(k)}(\bar{y}_j,\bar{w}_{jy})\bar{J}_{p_z(k)}(\bar{z}_j,\bar{w}_{jz}) \\
&= 2\Bigg[\bar{C}_{200}(2\bar{x}_j)(1)(1) + \bar{C}_{201}(2\bar{x}_j)(1)(\bar{z}_j) + \bar{C}_{220}(2\bar{x}_j)(\bar{y}_j^2+\frac{1}{2}w_{jy}^2)(1) \\
&\quad + \bar{C}_{202}(2\bar{x}_j)(1)(\bar{z}_j^2+\frac{1}{2}w_{jz}^2) + \bar{C}_{400}(4\bar{x}_j^3+6\bar{x}_j\bar{w}_{jx}^2)(1)(1)\Bigg] \\
&= 2\Bigg[\frac{1}{4}\bar{\omega}_0^2(2\bar{x}_j) + \frac{1}{4}\bar{\omega}_0^2\bar{b}(2\bar{x}_j)(\bar{z}_j) + \frac{1}{4}\bar{\omega}_0^2\bar{c}(2\bar{x}_j)(\bar{y}_j^2+\frac{1}{2}w_{jy}^2) \\
&\quad + \frac{1}{4}\bar{\omega}_0^2\bar{h}(2\bar{x}_j)(\bar{z}_j^2+\frac{1}{2}w_{jz}^2) + \frac{1}{8}\bar{\omega}_0^2\bar{c}(4\bar{x}_j^3+6\bar{x}_j\bar{w}_{jx}^2)\Bigg] \\
&= \bar{\omega}_0^2(\bar{x}_j) + \bar{\omega}_0^2\bar{b}(\bar{x}_j)(\bar{z}_j) + \bar{\omega}_0^2\bar{c}(\bar{y}_j^2+\frac{1}{2}w_{jy}^2)(\bar{x}_j) \\
&\quad + \bar{\omega}_0^2\bar{h}(\bar{z}_j^2+\frac{1}{2}w_{jz}^2)(\bar{x}_j) + \frac{1}{4}\bar{\omega}_0^2\bar{c}(4\bar{x}_j^3+6\bar{x}_j\bar{w}_{jx}^2)
\end{aligned}$$

the remaining derivatives can be determined in a similar fashion, then the center–coordinate equations of motion for the anharmonic potential have the following form (in scaled units):

$$\begin{aligned}
\ddot{\bar{x}}_j + (\bar{\omega}_0^2-\bar{\Omega}_z^2)\bar{x}_j &= +2\bar{\Omega}_z\dot{\bar{y}}_j - \bar{\omega}_0^2\bar{b}\bar{z}_j\bar{x}_j - \bar{\omega}_0^2\bar{c}(\bar{x}_j^2+\tfrac{3}{2}\bar{w}_{jx}^2)\bar{x}_j - \bar{\omega}_0^2\bar{c}(\bar{y}_j^2+\tfrac{1}{2}\bar{w}_{jy}^2)\bar{x}_j \\
&- \bar{\omega}_0^2\bar{h}(\bar{z}_j^2+\tfrac{1}{2}\bar{w}_{jz}^2)\bar{x}_j - F_{jx}(\bar{\mathbf{x}},\bar{\mathbf{w}}) \\
\ddot{\bar{y}}_j + (\bar{\omega}_0^2-\bar{\Omega}_z^2)\bar{y}_j &= -2\bar{\Omega}_z\dot{\bar{x}}_j - \bar{\omega}_0^2\bar{b}\bar{z}_j\bar{y}_j - \bar{\omega}_0^2\bar{c}(\bar{y}_j^2+\tfrac{3}{2}\bar{w}_{jy}^2)\bar{y}_j - \bar{\omega}_0^2\bar{c}(\bar{x}_j^2+\tfrac{1}{2}\bar{w}_{jx}^2)\bar{y}_j \\
&- \bar{\omega}_0^2\bar{h}(\bar{z}_j^2+\tfrac{1}{2}\bar{w}_{jz}^2)\bar{y}_j - F_{jy}(\bar{\mathbf{x}},\bar{\mathbf{w}}) \\
\ddot{\bar{z}}_j + \lambda^2\bar{\omega}_0^2\bar{z}_j &= -\tfrac{1}{2}\bar{\omega}_0^2\bar{b}(\bar{x}_j^2+\tfrac{1}{2}\bar{w}_{jx}^2) - \tfrac{1}{2}\bar{\omega}_0^2\bar{b}(\bar{y}_j^2+\tfrac{1}{2}\bar{w}_{jy}^2) - \bar{\omega}_0^2\bar{a}(\bar{z}_j^2+\tfrac{1}{2}\bar{w}_{jz}^2) \\
&- \bar{\omega}_0^2\bar{h}(\bar{x}_j^2+\tfrac{1}{2}\bar{w}_{jx}^2)\bar{z}_j - \bar{\omega}_0^2\bar{h}(\bar{y}_j^2+\tfrac{1}{2}\bar{w}_{jy}^2)\bar{z}_j - \bar{\omega}_0^2\bar{f}(\bar{z}_j^2+\tfrac{3}{2}\bar{w}_{jz}^2)\bar{z}_j \\
&- F_{jz}(\bar{\mathbf{x}},\bar{\mathbf{w}}) \\
j &= 1,\ldots,N_c
\end{aligned} \tag{72}$$

The EOMs for the widths are

$$\begin{aligned}
\ddot{\bar{w}}_{jx} + \bar{\omega}_0^2 \bar{w}_{jx} &= \frac{4}{\bar{w}_{jx}^3} + \frac{2\bar{g}N}{(2\pi)^{3/2}N_c}\left(\frac{1}{\bar{w}_{jx}\bar{w}_{jy}\bar{w}_{jz}\bar{w}_{jx}}\right) - \bar{\omega}_0^2 \bar{b}\bar{z}_j \bar{w}_{jx} \\
&- 3\bar{\omega}_0^2 \bar{c}(\bar{x}_j^2 + \tfrac{1}{2}\bar{w}_{jx}^2)\bar{w}_{jx} - \bar{\omega}_0^2 \bar{c}(\bar{y}_j^2 + \tfrac{1}{2}\bar{w}_{jy}^2)\bar{w}_{jx} \\
&- \bar{\omega}_0^2 \bar{h}(\bar{z}_j^2 + \tfrac{1}{2}\bar{w}_{jz}^2)\bar{w}_{jx} - W_{jx}(\bar{\mathbf{x}}, \bar{\mathbf{w}}) \\
\ddot{\bar{w}}_{jy} + \bar{\omega}_0^2 \bar{w}_{jy} &= \frac{4}{\bar{w}_{jy}^3} + \frac{2\bar{g}N}{(2\pi)^{3/2}N_c}\left(\frac{1}{\bar{w}_{jx}\bar{w}_{jy}\bar{w}_{jz}\bar{w}_{jy}}\right) - \bar{\omega}_0^2 \bar{b}\bar{z}_j \bar{w}_{jy} \\
&- 3\bar{\omega}_0^2 \bar{c}(\bar{y}_j^2 + \tfrac{1}{2}\bar{w}_{jy}^2)\bar{w}_{jy} - \bar{\omega}_0^2 \bar{c}(\bar{x}_j^2 + \tfrac{1}{2}\bar{w}_{jx}^2)\bar{w}_{jy} \\
&- \bar{\omega}_0^2 \bar{h}(\bar{z}_j^2 + \tfrac{1}{2}\bar{w}_{jz}^2)\bar{w}_{jy} - W_{jy}(\bar{\mathbf{x}}, \bar{\mathbf{w}}) \\
\ddot{\bar{w}}_{jz} + \lambda^2 \bar{\omega}_0^2 \bar{w}_{jz} &= \frac{4}{\bar{w}_{jz}^3} + \frac{2\bar{g}N}{(2\pi)^{3/2}N_c}\left(\frac{1}{\bar{w}_{jx}\bar{w}_{jy}\bar{w}_{jz}\bar{w}_{jz}}\right) - 2\bar{\omega}_0^2 \bar{a}\bar{z}_j \bar{w}_{jz} \\
&- 3\bar{\omega}_0^2 \bar{f}(\bar{z}_j^2 + \tfrac{1}{2}\bar{w}_{jz}^2)\bar{w}_{jz} - \bar{\omega}_0^2 \bar{h}(\bar{x}_j^2 + \tfrac{1}{2}\bar{w}_{jx}^2)\bar{w}_{jz} \\
&- \bar{\omega}_0^2 \bar{h}(\bar{y}_j^2 + \tfrac{1}{2}\bar{w}_{jy}^2)\bar{w}_{jz} - W_{jz}(\bar{\mathbf{x}}, \mathbf{w}) \\
j &= 1, \ldots, N_c
\end{aligned} \tag{73}$$

We again note here that the terms $F_{j\eta}(\bar{\mathbf{x}}, \bar{\mathbf{w}})$ and $W_{j\eta}(\bar{\mathbf{x}}, \bar{\mathbf{w}})$ account for interactions between different clouds and couple the widths and center coordinates of the j^{th} cloud to the widths and centers of all the other clouds. These terms are negligible unless cloud j has a spatial overlap with another cloud.

Our model is applied to the UVa interferometer sequence by utilizing the final values of the center coordinates and widths in one segment as the initial conditions for the following segment. For instance, prior to the first split, the initial conditions of the one–cloud ($N_c = 1$) model are

$$\bar{\eta}_1(0) = 0 \quad \text{and} \quad \bar{w}_{1\eta}(0) = \bar{w}_{\eta 0}; \quad \text{with} \quad \eta = x, y, z$$

Along with the initial condition for their derivatives

$$\dot{\bar{\eta}}_1(0) = 0 \quad \text{and} \quad \dot{\bar{w}}_{1\eta}(0) = 0$$

Physically, the undisturbed initial condensate should not move or change size. Hence we seek a stationary solution to the equations of motion so that $\dot{\bar{\eta}}_1(t) = 0$ and $\dot{\bar{w}}_{1\eta}(t) = 0$. From here, we see that any time later our values remain the same. Thus at time, $t = t_1$, when the first split occurs, our initial conditions are almost the same, except we need to account for the laser splitting the condensate. Given the figure 1, the initial split causes the cloud labeled 1 to move

in the $+y$ direction and the cloud labeled to moves in the $-y$ direction, so that

$$\dot{\bar{y}}_1(0) = +\bar{v}_B$$
$$\dot{\bar{y}}_2(0) = -\bar{v}_B$$

with the remaining initial conditions the same as in the previous segment. From here, the equations of motion for two–clouds can be used along with the initial conditions to compute the center coordinates and widths some time later. Once again, the final conditions of the two–cloud segment along with the effect of the laser splitting along the $\pm x$ direction are the initial conditions for the four–cloud segment in the UVa sequence. This is explored in detail later when considering the case of a harmonic potential with no cloud-cloud interactions.

4.5 Computing the fraction of stopped-atoms

To compute the fraction of stopped-atoms we need to determine the final state wavefunction. This can be done by evaluating Eq. (34) at time $t = t_2$, just before the final split, which can be written as

$$\begin{aligned}\Psi(\mathbf{r}, t_2) &= \frac{1}{2}\left(A_{11}(t)e^{g_{11}(\mathbf{r},t_2)} + A_{12}(t)e^{g_{12}(\mathbf{r},t_2)} + A_{21}(t)e^{g_{21}(\mathbf{r},t_2)} + A_{22}(t)e^{g_{22}(\mathbf{r},t_2)}\right) \\ &\equiv \psi_{11}(\mathbf{r}, t_2) + \psi_{12}(\mathbf{r}, t_2) + \psi_{21}(\mathbf{r}, t_2) + \psi_{22}(\mathbf{r}, t_2).\end{aligned}$$

where

$$g_{ij}(\mathbf{r}, t_2) \equiv \sum_{\substack{\eta=x,y,z \\ ij=\{11,12,21,22\}}} \left(-\frac{(\eta - \eta_{ij}(t_2))^2}{2(w_{ij\eta}(t_2))^2} + i\big(\epsilon_{ij\eta}(t_2)\eta + \beta_{ij}(t_2)\eta^2\big)\right);$$

and

$$\begin{aligned}\epsilon_{ijx}(t_2) &\equiv \frac{m}{\hbar}\left(\dot{x}_{ij}(t_2) - \Omega_z y_{ij}(t_2) - 4\beta_{ijx}(t_2)x_{ij}(t_2)\right) \\ \epsilon_{ijy}(t_2) &\equiv \frac{m}{\hbar}\left(\dot{y}_{ij}(t_2) + \Omega_z x_{ij}(t_2) - 4\beta_{ijy}(t_2)y_{ij}(t_2)\right) \\ \epsilon_{ijz}(t_2) &\equiv \frac{m}{\hbar}\left(\dot{z}_{ij}(t_2) - 4\beta_{ijz}(t_2)z_{ij}(t_2)\right).\end{aligned}$$

The first two terms, ψ_{11} and ψ_{12}, represent the two clouds in the plus (top) Sagnac interferometer shown in Fig. 1 while the last two terms, ψ_{21} and ψ_{22}, represent the clouds in the minus (bottom) Sagnac interferometer. Note, at $t = t_2$, the clouds in different interferometers have no spatial overlap and then product of their wavefunctions will be zero, hence we can treat the top and bottom interferometers separately. The final split has the effect of leaving half of cloud ij

unchanged and stopping the remaining half. In other words, it places cloud ij in an equal linear superposition of an unchanged wavefunction and one which is multiplied by a complex exponential. We can write this as,

$$\psi_{ij}(\mathbf{r},t_2) \rightarrow \frac{1}{\sqrt{2}}\left(\psi_{ij}(\mathbf{r},t_2) + \psi_{ij}(\mathbf{r},t_2)e^{-i\lambda_{ij}m\bar{v}_B\bar{x}/\hbar}\right)$$

where $\lambda_{11} = \lambda_{21} = -\lambda_{12} = -\lambda_{22} = 1$ accounts for which clouds travel along the $\pm x$ direction and the term with the exponential is the stopped cloud.

To compute the fraction of stopped atoms with this final state wavefunction we need to consider the probability of being in the zero–momentum state. In either interferometer, the contribution to this probability comes from the stopped clouds in that interferometer, so then we can write the fraction of stopped atoms as (in SI units),

$$S_+ = \int d^3r \left|\psi_{11}(\mathbf{r},t_2)e^{-imv_Bx/\hbar} + \psi_{12}(\mathbf{r},t_2)e^{+imv_Bx/\hbar}\right|^2$$

and

$$S_- = \int d^3r \left|\psi_{21}(\mathbf{r},t_2)e^{-imv_Bx/\hbar} + \psi_{22}(\mathbf{r},t_2)e^{+imv_Bx/\hbar}\right|^2$$

We can express $S_\pm$ in terms of the variational parameters by inserting the expression for the trial wave function into the above integrals and carrying out the integration. The expression for S_+ at time $t = t_2$ (in scaled units) is

$$\begin{aligned}
S_+ &\equiv \int d^3r \left|\psi_{11}(\bar{\mathbf{r}},\bar{t}_2)e^{-\frac{1}{2}i\bar{v}_B\bar{x}} + \psi_{12}(\bar{\mathbf{r}},\bar{t}_2)e^{+\frac{1}{2}i\bar{v}_B\bar{x}}\right|^2 \\
&= \int d^3r\Big(|\psi_{11}|^2 + |\psi_{12}|^2 + \psi_{11}^*\psi_{12}e^{i\bar{v}_B\bar{x}} + \psi_{11}\psi_{12}^*e^{-i\bar{v}_B\bar{x}}\Big) \\
&= \int d^3r\,|\psi_{11}|^2 + \int d^3r\,|\psi_{12}|^2 + \int d^3r\Big(\psi_{11}^*\psi_{12}e^{i\bar{v}_B\bar{x}} + \psi_{11}\psi_{12}^*e^{-i\bar{v}_B\bar{x}}\Big) \\
&= \frac{1}{4} + \frac{1}{4} + \int d^3r\Big(\psi_{11}^*\psi_{12}e^{i\bar{v}_B\bar{x}} + \psi_{11}\psi_{12}^*e^{-i\bar{v}_B\bar{x}}\Big) \\
&\equiv \frac{1}{2} + J_+ + J_+^* = \frac{1}{2} + 2\mathrm{Re}\left\{J_+\right\}
\end{aligned}$$

where

$$
\begin{aligned}
J_+ &\equiv \int d^3r \psi^*_{11}(\bar{\mathbf{r}},\bar{t}_2)\psi_{12}(\bar{\mathbf{r}},\bar{t}_2)e^{i\bar{v}_B\bar{x}} \\
&= \int d^3r \left(\frac{1}{2}A_{11}(\bar{t}_2)e^{g_{11}(\bar{\mathbf{r}},\bar{t}_2)}\right)^* \left(\frac{1}{2}A_{12}(\bar{t}_2)e^{g_{12}(\bar{\mathbf{r}},\bar{t}_2)}\right)e^{i\bar{v}_B\bar{x}} \\
&= \frac{1}{4}A^*_{11}(\bar{t}_2)A_{12}(\bar{t}_2)I_+ \\
&= \frac{1}{4}(\pi^{3/2}\bar{w}_{11x}(\bar{t}_2)\bar{w}_{11y}(\bar{t}_2)\bar{w}_{11z}(\bar{t}_2))^{-1/2} \\
&\times \ (\pi^{3/2}\bar{w}_{12x}(\bar{t}_2)\bar{w}_{12y}(\bar{t}_2)\bar{w}_{12z}(\bar{t}_2))^{-1/2}I_+
\end{aligned}
$$

where

$$
\begin{aligned}
I_+ &\equiv \int d^3r \ \exp\{g^*_{11}(\bar{\mathbf{r}},\bar{t}_2) + g_{12}(\bar{\mathbf{r}},\bar{t}_2) + i\bar{v}_B\bar{x}\} \\
&= \int d^3r \ \exp\left\{ \sum_{\eta=x,y,z}\left(-\frac{(\bar{\eta}-\bar{\eta}_{11})^2}{2(\bar{w}_{11\eta})^2} + i\big(\bar{\epsilon}_{11\eta}(\bar{t}_2)\bar{\eta} + \bar{\beta}_{11\eta}(\bar{t}_2)\bar{\eta}^2\big)\right)^* \right. \\
&+ \left. \sum_{\eta=x,y,z}\left(-\frac{(\bar{\eta}-\bar{\eta}_{12})^2}{2(\bar{w}_{12\eta})^2} + i\big(\bar{\epsilon}_{12\eta}(\bar{t}_2)\bar{\eta} + \bar{\beta}_{12\eta}(\bar{t}_2)\bar{\eta}^2\big)\right) + i\bar{v}_B\bar{x}\right\} \\
&= \int d^3r \ \exp\left\{ \sum_{\eta=x,y,z}\left(-\frac{(\bar{\eta}-\bar{\eta}_{11})^2}{2(\bar{w}_{11\eta})^2} - \frac{(\bar{\eta}-\bar{\eta}_{12})^2}{2(\bar{w}_{12\eta})^2} \right.\right. \\
&+ \left.\left. i\Big((\bar{\epsilon}_{12\eta}(\bar{t}_2) - \bar{\epsilon}_{11\eta}(\bar{t}_2))\bar{\eta} + (\bar{\beta}_{12\eta}(\bar{t}_2) - \bar{\beta}_{11\eta}(\bar{t}_2))\bar{\eta}^2\Big)\right) + i\bar{v}_B\bar{x}\right\} \\
&= \int_{-\infty}^{+\infty} d\bar{x} \exp\Big\{ -\frac{(\bar{x}-\bar{x}_{11})^2}{2(\bar{w}_{11x})^2} - \frac{(\bar{x}-\bar{x}_{12})^2}{2(\bar{w}_{12x})^2} \\
&+ i\Big((\bar{\epsilon}_{12x} - \bar{\epsilon}_{11x} + \bar{v}_B)\bar{x} + (\bar{\beta}_{12x} - \bar{\beta}_{11x})\bar{x}^2\Big)\Big\} \\
&\times \int_{-\infty}^{+\infty} d\bar{y} \exp\Big\{ -\frac{(\bar{y}-\bar{y}_{11})^2}{2(\bar{w}_{11y})^2} - \frac{(\bar{y}-\bar{y}_{12})^2}{2(\bar{w}_{12y})^2} \\
&+ i\Big((\bar{\epsilon}_{12y} - \bar{\epsilon}_{11y})\bar{y} + (\bar{\beta}_{12y} - \bar{\beta}_{11y})\bar{y}^2\Big)\Big\} \\
&\times \int_{-\infty}^{+\infty} d\bar{z} \exp\Big\{ -\frac{(\bar{z}-\bar{z}_{11})^2}{2(\bar{w}_{11z})^2} - \frac{(\bar{z}-\bar{z}_{12})^2}{2(\bar{w}_{12z})^2} \\
&+ i\Big((\bar{\epsilon}_{12z} - \bar{\epsilon}_{11z})\bar{z} + (\bar{\beta}_{12z} - \bar{\beta}_{11z})\bar{z}^2\Big)\Big\}
\end{aligned}
$$

we can relabel the integral terms for visual clarity and compute them below,

$$
\begin{aligned}
I_+ &\equiv K_+(\bar{x}_{11},\bar{w}_{11x},\bar{\epsilon}_{11x},\bar{\beta}_{11x},\bar{x}_{12},\bar{w}_{12x},\bar{\epsilon}_{12x}+\bar{v}_B,\bar{\beta}_{12x}) \\
&\times K_+(\bar{y}_{11},\bar{w}_{11y},\bar{\epsilon}_{11y},\bar{\beta}_{11y},\bar{y}_{12},\bar{w}_{12y},\bar{\epsilon}_{12y},\bar{\beta}_{12y}) \\
&\times K_+(\bar{z}_{11},\bar{w}_{11z},\bar{\epsilon}_{11z},\bar{\beta}_{11z},\bar{z}_{12},\bar{w}_{12z},\bar{\epsilon}_{12z},\bar{\beta}_{12z})
\end{aligned}
$$

where $K_+(\bar{\eta}_{11}, \bar{w}_{11\eta}, \bar{\epsilon}_{11\eta}, \bar{\beta}_{11\eta}, \bar{\eta}_{12}, \bar{w}_{12\eta}, \bar{\epsilon}_{12\eta}, \bar{\beta}_{12\eta})$ is

$$\begin{aligned}
K_+ &\equiv \int_{-\infty}^{+\infty} d\bar{\eta} \exp\Big\{ -\frac{(\bar{\eta}-\bar{\eta}_{11})^2}{2\bar{w}_{11\eta}^2} - \frac{(\bar{\eta}-\bar{\eta}_{12})^2}{2\bar{w}_{12}^2} \\
&+ i\Big((\bar{\epsilon}_{12\eta}-\bar{\epsilon}_{11\eta})\bar{\eta} + (\bar{\beta}_{12\eta}-\bar{\beta}_{11\eta})\bar{\eta}^2\Big)\Big\} \\
&= \pi^{1/2} \frac{\exp\left\{ \frac{\left(\frac{\bar{\eta}_{11}}{2\bar{w}_{11\eta}^2} + \frac{\bar{\eta}_2}{2\bar{w}_{12\eta}^2} + \frac{1}{2}i(\bar{\epsilon}_{12\eta}-\bar{\epsilon}_{11\eta})\right)^2}{\left(\frac{1}{2\bar{w}_{11\eta}^2} + \frac{1}{2\bar{w}_{12\eta}^2} - i(\bar{\beta}_{12\eta}-\bar{\beta}_{11\eta})\right)} - \left(\frac{\bar{\eta}_{11\eta}^2}{2\bar{w}_{11\eta}^2} + \frac{\bar{\eta}_{12\eta}^2}{2\bar{w}_{12\eta}^2}\right)\right\}}{\left(\frac{1}{2\bar{w}_{11\eta}^2} + \frac{1}{2\bar{w}_{12\eta}^2} - i(\bar{\beta}_{12\eta}-\bar{\beta}_{11\eta})\right)^{1/2}} \\
&= \pi^{1/2}\bar{w}_{11\eta}^{1/2}\bar{w}_{12\eta}^{1/2} \frac{\exp\left\{ \frac{\left(\frac{\bar{\eta}_{11}}{2\bar{w}_{11\eta}^2} + \frac{\bar{\eta}_{12}}{2\bar{w}_{12\eta}^2} + \frac{1}{2}i(\bar{\epsilon}_{12\eta}-\bar{\epsilon}_{11\eta})\right)^2}{\left(\frac{1}{2\bar{w}_{11\eta}^2} + \frac{1}{2\bar{w}_{12\eta}^2} - i(\bar{\beta}_{12\eta}-\bar{\beta}_{11\eta})\right)} - \left(\frac{\bar{\eta}_{11}^2}{2\bar{w}_{11\eta}^2} + \frac{\bar{\eta}_{12}^2}{2\bar{w}_{12\eta}^2}\right)\right\}}{\left(\frac{\bar{w}_{12\eta}}{2\bar{w}_{11\eta}} + \frac{\bar{w}_{11\eta}}{2\bar{w}_{12\eta}} - i(\bar{\beta}_{12\eta}-\bar{\beta}_{11\eta})\bar{w}_{11\eta}\bar{w}_{12\eta}\right)^{1/2}} \\
&= \pi^{1/2}\bar{w}_{11\eta}^{1/2}\bar{w}_{12\eta}^{1/2} M(\bar{\eta}_{11}, \bar{w}_{11\eta}, \bar{\epsilon}_{11\eta}, \bar{\beta}_{11\eta}, \bar{\eta}_{12}, \bar{w}_{12\eta}, \bar{\epsilon}_{12\eta}, \bar{\beta}_{12\eta})
\end{aligned}$$

(noting that when $\bar{\eta} = \bar{x}$, we have $\bar{\epsilon}_{12\eta} = \bar{\epsilon}_{12x} + \bar{v}_B$) and where M is defined as follows

$$M \equiv \frac{\exp\left\{ \frac{\left(\frac{\bar{\eta}_{11}}{2\bar{w}_{11\eta}^2} + \frac{\bar{\eta}_{12}}{2\bar{w}_{12\eta}^2} + \frac{1}{2}i(\bar{\epsilon}_{12\eta}-\bar{\epsilon}_{11\eta})\right)^2}{\left(\frac{1}{2\bar{w}_{11\eta}^2} + \frac{1}{2\bar{w}_{12\eta}^2} - i(\bar{\beta}_{12\eta}-\bar{\beta}_{11\eta})\right)} - \left(\frac{\bar{\eta}_{11}^2}{2\bar{w}_{11\eta}^2} + \frac{\bar{\eta}_{12}^2}{2\bar{w}_{12\eta}^2}\right)\right\}}{\left(\frac{\bar{w}_{12\eta}}{2\bar{w}_{11\eta}} + \frac{\bar{w}_{11\eta}}{2\bar{w}_{12\eta}} - i(\bar{\beta}_{12\eta}-\bar{\beta}_{11\eta})\bar{w}_{11\eta}\bar{w}_{12\eta}\right)^{1/2}}$$

since M is dimensionless, it yields an equivalent expression in SI units (where $v_B \to \frac{mv_B}{\hbar}$).

Hence we can write I_+ in terms of M as

$$\begin{aligned}
I_+ &= \pi^{3/2}(\bar{w}_{11x}\bar{w}_{12x}\bar{w}_{11y}\bar{w}_{12y}\bar{w}_{11z}\bar{w}_{12z})^{1/2} \\
&\times M(x_{11}, w_{11x}, \epsilon_{11x}, \beta_{11x}, x_{12}, w_{12x}, \epsilon_{12x} + \tfrac{mv_B}{\hbar}, \beta_{12x}) \\
&\times M(y_{11}, w_{11y}, \epsilon_{11y}, \beta_{11y}, y_{12}, w_{12y}, \epsilon_{12y}, \beta_{12y}) \\
&\times M(z_{11}, w_{11z}, \epsilon_{11z}, \beta_{11z}, z_{12}, w_{12z}, \epsilon_{12z}, \beta_{12z})
\end{aligned}$$

Writing J_+ in terms of the M factors we have,

$$\begin{aligned}
J_+ &= \frac{1}{4} M(x_{11}, w_{11x}, \epsilon_{11x}, \beta_{11x}, x_{12}, w_{12x}, \epsilon_{12x} + \tfrac{mv_B}{\hbar}, \beta_{12x}) \\
&\times M(y_{11}, w_{11y}, \epsilon_{11y}, \beta_{11y}, y_{12}, w_{12y}, \epsilon_{12y}, \beta_{12y}) \\
&\times M(z_{11}, w_{11z}, \epsilon_{11z}, \beta_{11z}, z_{12}, w_{12z}, \epsilon_{12z}, \beta_{12z})
\end{aligned}$$

Finally we can write S_+ as (in SI units),

$$\begin{aligned} S_+ &= \frac{1}{2} + \frac{1}{2}\mathrm{Re}\Big\{ M(x_{11}(t_2), w_{11x}(t_2), \epsilon_{11x}(t_2), \beta_{11x}(t_2), \\ &\quad x_{12}(t_2), w_{12x}(t_2), \epsilon_{12x}(t_2) + \tfrac{Mv_B}{\hbar}, \beta_{12x}(t_2)) \\ &\times M(y_{11}(t_2), w_{11y}(t_2), \epsilon_{11y}(t_2), \beta_{11y}(t_2), \\ &\quad y_{12}(t_2), w_{12y}(t_2), \epsilon_{12y}(t_2), \beta_{12y}(t_2)) \\ &\times M(z_{11}(t_2), w_{11z}(t_2), \epsilon_{11z}(t_2), \beta_{11z}(t_2), \\ &\quad z_{12}(t_2), w_{12z}(t_2), \epsilon_{12z}(t_2), \beta_{12z}(t_2)) \Big\} \end{aligned} \tag{74}$$

$$\begin{aligned} S_- &= \frac{1}{2} + \frac{1}{2}\mathrm{Re}\Big\{ M(x_{21}(t_2), w_{21x}(t_2), \epsilon_{21x}(t_2), \beta_{21x}(t_2), \\ &\quad x_{22}(t_2), w_{22x}(t_2), \epsilon_{22x}(t_2) + \tfrac{Mv_B}{\hbar}, \beta_{22x}(t_2)) \\ &\times M(y_{21}(t_2), w_{21y}(t_2), \epsilon_{21y}(t_2), \beta_{21y}(t_2), \\ &\quad y_{22}(t_2), w_{22y}(t_2), \epsilon_{22y}(t_2), \beta_{22y}(t_2)) \\ &\times M(z_{21}(t_2), w_{21z}(t_2), \epsilon_{21z}(t_2), \beta_{21z}(t_2), \\ &\quad z_{22}(t_2), w_{22z}(t_2), \epsilon_{22z}(t_2), \beta_{22z}(t_2)) \Big\} \end{aligned} \tag{75}$$

Using these we can compute $S_\pm$ in terms of the values of the variational parameters just before the final split along with the effect of the split changing the phase.

4.5.1 Expression for S_+ at zero rotation speed

An approximate expression for S_+ in the case of the anharmonic potential can be determined by neglecting cloud–cloud interactions and setting the rotating–frame speed to zero ($\Omega_z = 0$). We can further simplify by utilizing the symmetries of the solutions for this case. Namely that clouds within an interferometer have oppositely orientated x and $\dot{x}$, similarly orientated y and $\dot{y}$ along with z and $\dot{z}$. Quantitatively we have,

$$x_{11}(t) \equiv x_1(t), \quad x_{12}(t) \equiv x_2(t), \quad x_1(t) = -x_2(t), \quad \dot{x}_1(t) = -\dot{x}_2(t)$$

$$y_{11}(t) = y_{12}(t), \quad \dot{y}_{11}(t) = \dot{y}_{12}(t), \quad z_{11}(t) = z_{12}(t), \quad \dot{z}_{11}(t) = \dot{z}_{12}(t),$$

Furthermore all of the x and y widths and their dots for both clouds are the same at all times:

$$w_{11x}(t) = w_{12x}(t) = w_{11y}(t) = w_{12y}(t) \equiv w_\perp(t)$$

$$\dot{w}_{11x}(t) = \dot{w}_{12x}(t) = \dot{w}_{11y}(t) = \dot{w}_{12y}(t) \equiv \dot{w}_\perp(t)$$

Also, the z widths and dot widths of the two clouds are equal

$$w_{11z}(t) = w_{12z}(t) \equiv w_z(t), \quad \text{and} \quad \dot{w}_{11z}(t) = \dot{w}_{12z}(t) \equiv \dot{w}_z(t)$$

The width symmetries also include the $\beta = \dot{w}/(4w)$ factors. Thus

$$\bar{\beta}^{(4)}_{11x}(t) = \bar{\beta}^{(4)}_{12x}(t) = \bar{\beta}^{(4)}_{11y}(t) = \bar{\beta}^{(4)}_{12y}(t) \equiv \beta_\perp(t)$$

$$\bar{\beta}^{(4)}_{11z}(t) = \bar{\beta}^{(4)}_{12z}(t) \equiv \beta_z(t)$$

Since we're considering just the top interferomter, we can write the expression for S_+ as,

$$S_+ = \frac{1}{2} + \frac{1}{2}\mathrm{Re}\Big\{M_x M_y M_z\Big\}$$

Now let's consider the factor M_x. We have

$$\begin{aligned}
M_x &\equiv M(\bar{x}^{(4)}_{11}(t_2), \bar{w}^{(4)}_{11x}(t_2), \bar{\epsilon}^{(4)}_{11x}(t_2), \bar{\beta}^{(4)}_{11x}(t_2), \bar{x}^{(4)}_{12}(t_2), \bar{w}^{(4)}_{12x}(t_2), \bar{\epsilon}^{(4)}_{12x}(t_2) + \bar{v}_B, \bar{\beta}^{(4)}_{12x}(t_2)) \\
&= M(x_1(t_2), w_\perp(t_2), \epsilon_{1x}(t_2), \beta_\perp(t_2), -x_1(t_2), w_\perp(t_2), \epsilon_{2x}(t_2), \beta_\perp(t_2)) \\
&= \frac{\exp\left\{ \frac{\left(\frac{x_1}{2w_\perp^2} + \frac{-x_1}{2w_\perp^2} + \frac{1}{2}i(\epsilon_2 - \epsilon_1)\right)^2}{\left(\frac{1}{2w_\perp^2} + \frac{1}{2w_\perp^2} - i(\beta_\perp - \beta_\perp)\right)} - \left(\frac{x_1^2}{2w_\perp^2} + \frac{x_2^2}{2w_\perp^2}\right) \right\}}{\left(\frac{w_\perp}{2w_\perp} + \frac{w_\perp}{2w_\perp} - i(\beta_\perp - \beta_\perp)w_\perp w_\perp\right)^{1/2}} \\
&= \exp\left\{ -\frac{1}{4}(\epsilon_{2x} - \epsilon_{1x})^2 w_\perp^2 - \left(\frac{x_1^2}{2w_\perp^2} + \frac{x_2^2}{2w_\perp^2}\right) \right\}
\end{aligned}$$

noting that we've evaluated the time dependent parameters at $t = t_2$. Finally we consider factor $\epsilon_{2x} - \epsilon_{1x}$ for the case where the rotation speed is zero ($\bar{\Omega}_z = 0$)

$$\begin{aligned}
\epsilon_{2x} - \epsilon_{1x} &= \left(\bar{\epsilon}^{(4)}_{12x}(t_2) + \bar{v}_B\right) - \bar{\epsilon}^{(4)}_{11x}(t_2) \\
&= (\tfrac{1}{2}\dot{\bar{x}}^{(4)}_{12}(\bar{t}_2) - 2\bar{\beta}^{(4)}_{12x}(\bar{t}_2)\bar{x}^{(4)}_{12}(\bar{t}_2)) + \bar{v}_B - (\tfrac{1}{2}\dot{\bar{x}}^{(4)}_{11}(\bar{t}_2) - 2\bar{\beta}^{(4)}_{11x}(\bar{t}_2)\bar{x}^{(4)}_{11}(\bar{t}_2)) \\
&= (\tfrac{1}{2}\dot{x}_2 - 2\beta_\perp x_2) + \bar{v}_B - (\tfrac{1}{2}\dot{x}_1 - 2\beta_\perp x_1) \\
&= \tfrac{1}{2}\dot{x}_2 - 2\beta_\perp x_2 + \bar{v}_B - \tfrac{1}{2}\dot{x}_1 + 2\beta_\perp x_1 \\
&= \bar{v}_B - \tfrac{1}{2}(\dot{x}_1 - \dot{x}_2) + 2\beta_\perp(x_1 - x_2)
\end{aligned}$$

We insert this into the expression for M_x to get

$$\begin{aligned} M_x &= \exp\left\{ -\frac{1}{4}\Big(\big(\bar{v}_B - \tfrac{1}{2}(\dot{\bar{x}}_1 - \dot{\bar{x}}_2)\big) + 2\bar{\beta}_\perp(\bar{x}_1 - \bar{x}_2)\Big)^2 w_\perp^2 - \Big(\frac{x_1^2}{2w_\perp^2} + \frac{x_2^2}{2w_\perp^2}\Big)\right\} \\ &= \exp\left\{ -\left(\frac{M}{\hbar}\right)^2 \big[\tfrac{1}{2}\big(2v_B - (\dot{x}_1 - \dot{x}_2)\big)w_\perp + (x_1 - x_2)\dot{w}_\perp\big]^2 - \Big(\frac{x_1^2}{2w_\perp^2} + \frac{x_2^2}{2w_\perp^2}\Big)\right\} \end{aligned}$$

Symmetries could be used to further simplify this expression, however this form will be useful for providing a physical interpretation of this factor. Carrying out a similar procedure for the factors M_y and M_z, we find

$$\begin{aligned} M_y &= \exp\left\{ \Big(\frac{y_1}{w_\perp^2} + \tfrac{1}{2}i(\epsilon_{2y} - \epsilon_{1y})\Big)^2 w_\perp^2 - \frac{y_1^2}{w_\perp^2}\right\} \\ &= \exp\left\{ \Big(\frac{y_1}{w_\perp^2}\Big)^2 w_\perp^2 - \frac{y_1^2}{w_\perp^2}\right\} \\ M_y &= 1 \end{aligned}$$

and

$$\begin{aligned} M_z &= \exp\left\{ \Big(\frac{z_1}{w_z^2} + \tfrac{1}{2}i(\epsilon_{2z} - \epsilon_{1z})\Big)^2 w_z^2 - \frac{z_1^2}{w_z^2}\right\} \\ &= \exp\left\{ \Big(\frac{z_1}{w_z^2}\Big)^2 w_z^2 - \frac{z_1^2}{w_z^2}\right\} \\ M_z &= 1 \end{aligned}$$

The final expression for S_+ for the case of an anharmonic potential when the rotation speed is zero can be written as

$$\begin{aligned} S_+ &= \tfrac{1}{2} + \tfrac{1}{2}\mathrm{Re}\Big\{M_x M_y M_z\Big\} \\ &= \tfrac{1}{2} + \tfrac{1}{2}\exp\left\{ -\frac{1}{4}\Big(\big(\bar{v}_B - \tfrac{1}{2}(\dot{\bar{x}}_1 - \dot{\bar{x}}_2)\big) + 2\bar{\beta}_\perp(\bar{x}_1 - \bar{x}_2)\Big)^2 \bar{w}_\perp^2 \right. \\ &- \left. \Big(\frac{\bar{x}_1^2}{2\bar{w}_\perp^2} + \frac{\bar{x}_2^2}{2\bar{w}_\perp^2}\Big)\right\}. \end{aligned} \tag{76}$$

4.6 Exact expression for S_+ for non–interacting clouds in a harmonic potential

The variational equations of motion in the rotating frame for a harmonic potential with cloud-cloud interactions neglected have the form,

$$\begin{aligned}
\ddot{\bar{x}}_j + (\bar{\omega}_0^2 - \bar{\Omega}_z^2)\bar{x}_j &= +2\bar{\Omega}_z\dot{\bar{y}}_j \\
\ddot{\bar{y}}_j + (\bar{\omega}_0^2 - \bar{\Omega}_z^2)\bar{y}_j &= -2\bar{\Omega}_z\dot{\bar{x}}_j \\
\ddot{\bar{z}}_j + \lambda^2\bar{\omega}_0^2\bar{z}_j &= 0 \\
\ddot{\bar{w}}_{jx} + \bar{\omega}_0^2\bar{w}_{jx} &= \frac{4}{\bar{w}_{jx}^3} + \frac{2\bar{g}N}{(2\pi)^{3/2}N_c}\left(\frac{1}{\bar{w}_{jx}\bar{w}_{jy}\bar{w}_{jz}\bar{w}_{jx}}\right) \\
\ddot{\bar{w}}_{jy} + \bar{\omega}_0^2\bar{w}_{jy} &= \frac{4}{\bar{w}_{jy}^3} + \frac{2\bar{g}N}{(2\pi)^{3/2}N_c}\left(\frac{1}{\bar{w}_{jx}\bar{w}_{jy}\bar{w}_{jz}\bar{w}_{jy}}\right) \\
\ddot{\bar{w}}_{jz} + \lambda^2\bar{\omega}_0^2\bar{w}_{jz} &= \frac{4}{\bar{w}_{jz}^3} + \frac{2\bar{g}N}{(2\pi)^{3/2}N_c}\left(\frac{1}{\bar{w}_{jx}\bar{w}_{jy}\bar{w}_{jz}\bar{w}_{jz}}\right) \\
j &= 1, \ldots, N_c.
\end{aligned} \tag{77}$$

The equations for the center coordinates of each cloud form a closed set and can be solved exactly. The width equations must be solved numerically but exhibit a clear symmetry in that the equations for $w_{jx}(t)$ and $w_{jy}(t)$ are the same. When the initial conditions for these widths are the same (as is the case when applying the one, two, and four–cloud models to the UVa AI sequence) the solutions $w_{jx}(t)$ and $w_{jy}(t)$ will be identical. Note that the evolution of the widths do not depend on the speed, Ω_z, of the rotating frame as this does not appear in the width equations of motion.

The solutions to the center coordinates are given below. If we know the initial conditions at time t_0, namely

$$x(t_0), \quad \dot{x}(t_0), \quad y(t_0), \quad \dot{y}(t_0), \quad z(t_0), \quad \dot{z}(t_0), \quad \omega, \quad \lambda, \quad \text{and} \quad \Omega$$

then these quantities at time t are given by

$$\begin{aligned} x(t) &= x(t_0)\cos(\omega(t-t_0))\cos(\Omega(t-t_0)) \\ &+ \frac{1}{\omega}\left(\dot{x}(t_0)-\Omega y(t_0)\right)\sin(\omega(t-t_0))\cos(\Omega(t-t_0)) \\ &+ y(t_0)\cos(\omega(t-t_0))\sin(\Omega(t-t_0)) \\ &+ \frac{1}{\omega}\left(\dot{y}(t_0)+\Omega x(t_0)\right)\sin(\omega(t-t_0))\sin(\Omega(t-t_0)) \end{aligned} \tag{78}$$

$$\begin{aligned} y(t) &= -x(t_0)\cos(\omega(t-t_0))\sin(\Omega(t-t_0)) \\ &- \frac{1}{\omega}\left(\dot{x}(t_0)-\Omega y(t_0)\right)\sin(\omega(t-t_0))\sin(\Omega(t-t_0)) \\ &+ y(t_0)\cos(\omega(t-t_0))\cos(\Omega(t-t_0)) \\ &+ \frac{1}{\omega}\left(\dot{y}(t_0)+\Omega x(t_0)\right)\sin(\omega(t-t_0))\cos(\Omega(t-t_0)) \end{aligned} \tag{79}$$

$$z(t) = z(t_0)\cos(\lambda\omega(t-t_0)) + \left(\frac{\dot{z}(t_0)}{\lambda\omega}\right)\sin(\lambda\omega(t-t_0)) \tag{80}$$

and

$$\begin{aligned} \dot{x}(t) &= -\left(\frac{\Omega}{\omega}\left(\dot{x}(t_0)-\Omega y(t_0)\right)+\omega y(t_0)\right)\sin(\omega(t-t_0))\sin(\Omega(t-t_0)) \\ &+ \left(\frac{\Omega}{\omega}\left(\dot{y}(t_0)+\Omega x(t_0)\right)-\omega x(t_0)\right)\sin(\omega(t-t_0))\cos(\Omega(t-t_0)) \\ &+ \dot{y}(t_0)\cos(\omega(t-t_0))\sin(\Omega(t-t_0)) \\ &+ \dot{x}(t_0)\cos(\omega(t-t_0))\cos(\Omega(t-t_0)) \end{aligned} \tag{81}$$

$$\begin{aligned} \dot{y}(t) &= -\left(\frac{\Omega}{\omega}\left(\dot{y}(t_0)+\Omega x(t_0)\right)-\omega x(t_0)\right)\sin(\omega(t-t_0))\sin(\Omega(t-t_0)) \\ &- \left(\frac{\Omega}{\omega}\left(\dot{x}(t_0)-\Omega y(t_0)\right)+\omega y(t_0)\right)\sin(\omega(t-t_0))\cos(\Omega(t-t_0)) \\ &- \dot{x}(t_0)\cos(\omega(t-t_0))\sin(\Omega(t-t_0)) \\ &+ \dot{y}(t_0)\cos(\omega(t-t_0))\cos(\Omega(t-t_0)) \end{aligned} \tag{82}$$

$$\dot{z}(t) = -\lambda\omega z(t_0)\sin(\lambda\omega(t-t_0)) + \dot{z}(t_0)\cos(\lambda\omega(t-t_0)) \tag{83}$$

As mentioned previously, the final conditions of one segment of the AI sequence along with the effect of splitting provide the initial conditions for the following segment. In this case, the final conditions of the two–cloud segment give the initial conditions of the four–cloud segment. The

initial conditions for clouds 11 and 12 in the four–cloud model are

$$\begin{aligned}
\bar{x}_{11}^{(4)}(\bar{t}_1) = \bar{x}_{12}^{(4)}(\bar{t}_1) &= \frac{\bar{v}_B}{\bar{\omega}_0}\sin\big((\pi/2)(\bar{\Omega}_z/\bar{\omega}_0)\big) \\
\bar{y}_{11}^{(4)}(\bar{t}_1) = \bar{y}_{12}^{(4)}(\bar{t}_1) &= \frac{\bar{v}_B}{\bar{\omega}_0}\cos\big((\pi/2)(\bar{\Omega}_z/\bar{\omega}_0)\big) \\
\bar{z}_{11}^{(4)}(\bar{t}_1) = \bar{z}_{12}^{(4)}(\bar{t}_1) &= 0 \\
\dot{\bar{x}}_{11}^{(4)}(\bar{t}_1) &= \left(\frac{\bar{\Omega}_z}{\bar{\omega}_0}\right)\bar{v}_B\cos\big((\pi/2)(\bar{\Omega}_z/\bar{\omega}_0)\big) + \bar{v}_B \\
\dot{\bar{x}}_{12}^{(4)}(\bar{t}_1) &= \left(\frac{\bar{\Omega}_z}{\bar{\omega}_0}\right)\bar{v}_B\cos\big((\pi/2)(\bar{\Omega}_z/\bar{\omega}_0)\big) - \bar{v}_B \\
\dot{\bar{y}}_{11}^{(4)}(\bar{t}_1) = \dot{\bar{y}}_{12}^{(4)}(\bar{t}_1) &= -\left(\frac{\bar{\Omega}_z}{\bar{\omega}_0}\right)\bar{v}_B\sin\big((\pi/2)(\bar{\Omega}_z/\bar{\omega}_0)\big) \\
\dot{\bar{z}}_{11}^{(4)}(\bar{t}_1) = \dot{\bar{z}}_{12}^{(4)}(\bar{t}_1) &= 0
\end{aligned}$$

and the initial conditions for clouds 21 and 22 are

$$\begin{aligned}
\bar{x}_{21}^{(4)}(\bar{t}_1) = \bar{x}_{22}^{(4)}(\bar{t}_1) &= -\frac{\bar{v}_B}{\bar{\omega}_0}\sin\big((\pi/2)(\bar{\Omega}_z/\bar{\omega}_0)\big) \\
\bar{y}_{21}^{(4)}(\bar{t}_1) = \bar{y}_{22}^{(4)}(\bar{t}_1) &= -\frac{\bar{v}_B}{\bar{\omega}_0}\cos\big((\pi/2)(\bar{\Omega}_z/\bar{\omega}_0)\big) \\
\bar{z}_{21}^{(4)}(\bar{t}_1) = \bar{z}_{22}^{(4)}(\bar{t}_1) &= 0 \\
\dot{\bar{x}}_{21}^{(4)}(\bar{t}_1) &= -\left(\frac{\bar{\Omega}_z}{\bar{\omega}_0}\right)\bar{v}_B\cos\big((\pi/2)(\bar{\Omega}_z/\bar{\omega}_0)\big) + \bar{v}_B \\
\dot{\bar{x}}_{22}^{(4)}(\bar{t}_1) &= -\left(\frac{\bar{\Omega}_z}{\bar{\omega}_0}\right)\bar{v}_B\cos\big((\pi/2)(\bar{\Omega}_z/\bar{\omega}_0)\big) - \bar{v}_B \\
\dot{\bar{y}}_{21}^{(4)}(\bar{t}_1) = \dot{\bar{y}}_{22}^{(4)}(\bar{t}_1) &= \left(\frac{\bar{\Omega}_z}{\bar{\omega}_0}\right)\bar{v}_B\sin\big((\pi/2)(\bar{\Omega}_z/\bar{\omega}_0)\big) \\
\dot{\bar{z}}_{21}^{(4)}(\bar{t}_1) = \dot{\bar{z}}_{22}^{(4)}(\bar{t}_1) &= 0
\end{aligned}$$

We can use these initial conditions for the four–cloud model to along with Eqs. (78), (79), (81), and (82) to determine the position and velocities of a cloud at time $\bar{t} = \bar{t}_2$. In this case, we want the values just before the final split. This occurs after the clouds have orbited for one harmonic trap period, $\bar{T}$. Hence $\bar{t}_2 = \bar{t}_1 + \bar{T}$. In these equations we take $t_0 = \bar{t}_1$, $\omega(t - t_0) = \bar{\omega}_0(\bar{t}_2 - \bar{t}_1) = \bar{\omega}_0\bar{T} = 2\pi$ and $\Omega(t - t_0) = \bar{\Omega}_z(\bar{t}_2 - \bar{t}_1) = \bar{\Omega}_z\bar{T} = (2\pi)(\bar{\Omega}_z/\bar{\omega}_0)$.

$$\begin{aligned}
\bar{x}(\bar{t}_2) &= \bar{x}(\bar{t}_1)\cos\big(2\pi(\bar{\Omega}_z/\bar{\omega}_0)\big) + \bar{y}(\bar{t}_1)\sin\big(2\pi(\bar{\Omega}_z/\bar{\omega}_0)\big) \\
\bar{y}(\bar{t}_2) &= -\bar{x}(\bar{t}_1)\sin\big(2\pi(\bar{\Omega}_z/\bar{\omega}_0)\big) + \bar{y}(\bar{t}_1)\cos\big(2\pi(\bar{\Omega}_z/\bar{\omega}_0)\big) \\
\dot{\bar{x}}(\bar{t}_2) &= \dot{\bar{y}}(\bar{t}_1)\sin\big(2\pi(\bar{\Omega}_z/\bar{\omega}_0)\big) + \dot{\bar{x}}(\bar{t}_1)\cos\big(2\pi(\bar{\Omega}_z/\bar{\omega}_0)\big) \\
\dot{\bar{y}}(\bar{t}_2) &= -\dot{\bar{x}}(\bar{t}_1)\sin\big(2\pi(\bar{\Omega}_z/\bar{\omega}_0)\big) + \dot{\bar{y}}(\bar{t}_1)\cos\big(2\pi(\bar{\Omega}_z/\bar{\omega}_0)\big)
\end{aligned}$$

By substituting our initial conditions the solutions for the clouds in the top interferometer (11

and 12), we have

$$
\begin{aligned}
\bar{x}_{11}^{(4)}(\bar{t}_2) = \bar{x}_{12}^{(4)}(\bar{t}_2) &= \frac{\bar{v}_B}{\bar{\omega}_0}\sin\big((\pi/2)(\bar{\Omega}_z/\bar{\omega}_0)\big)\cos\big(2\pi(\bar{\Omega}_z/\bar{\omega}_0)\big) \\
&+ \frac{\bar{v}_B}{\bar{\omega}_0}\cos\big((\pi/2)(\bar{\Omega}_z/\bar{\omega}_0)\big)\sin\big(2\pi(\bar{\Omega}_z/\bar{\omega}_0)\big) \\
\bar{y}_{11}^{(4)}(\bar{t}_2) = \bar{y}_{12}^{(4)}(\bar{t}_2) &= -\frac{\bar{v}_B}{\bar{\omega}_0}\sin\big((\pi/2)(\bar{\Omega}_z/\bar{\omega}_0)\big)\sin\big(2\pi(\bar{\Omega}_z/\bar{\omega}_0)\big) \\
&+ \frac{\bar{v}_B}{\bar{\omega}_0}\cos\big((\pi/2)(\bar{\Omega}_z/\bar{\omega}_0)\big)\cos\big(2\pi(\bar{\Omega}_z/\bar{\omega}_0)\big) \\
\bar{z}_{11}^{(4)}(\bar{t}_2) = \bar{z}_{12}^{(4)}(\bar{t}_2) &= 0 \\
\dot{\bar{x}}_{11}^{(4)}(\bar{t}_2) &= -\left(\frac{\bar{\Omega}_z}{\bar{\omega}_0}\right)\bar{v}_B\sin\big((\pi/2)(\bar{\Omega}_z/\bar{\omega}_0)\big)\sin\big(2\pi(\bar{\Omega}_z/\bar{\omega}_0)\big) \\
&+ \left(\left(\frac{\bar{\Omega}_z}{\bar{\omega}_0}\right)\bar{v}_B\cos\big((\pi/2)(\bar{\Omega}_z/\bar{\omega}_0)\big) + \bar{v}_B\right)\cos\big(2\pi(\bar{\Omega}_z/\bar{\omega}_0)\big) \\
\dot{\bar{x}}_{12}^{(4)}(\bar{t}_2) &= -\left(\frac{\bar{\Omega}_z}{\bar{\omega}_0}\right)\bar{v}_B\sin\big((\pi/2)(\bar{\Omega}_z/\bar{\omega}_0)\big)\sin\big(2\pi(\bar{\Omega}_z/\bar{\omega}_0)\big) \\
&+ \left(\left(\frac{\bar{\Omega}_z}{\bar{\omega}_0}\right)\bar{v}_B\cos\big((\pi/2)(\bar{\Omega}_z/\bar{\omega}_0)\big) - \bar{v}_B\right)\cos\big(2\pi(\bar{\Omega}_z/\bar{\omega}_0)\big) \\
\dot{\bar{y}}_{11}^{(4)}(\bar{t}_2) &= -\left(\left(\frac{\bar{\Omega}_z}{\bar{\omega}_0}\right)\bar{v}_B\cos\big((\pi/2)(\bar{\Omega}_z/\bar{\omega}_0)\big) + \bar{v}_B\right)\sin\big(2\pi(\bar{\Omega}_z/\bar{\omega}_0)\big) \\
&- \left(\frac{\bar{\Omega}_z}{\bar{\omega}_0}\right)\bar{v}_B\sin\big((\pi/2)(\bar{\Omega}_z/\bar{\omega}_0)\big)\cos\big(2\pi(\bar{\Omega}_z/\bar{\omega}_0)\big) \\
\dot{\bar{y}}_{12}^{(4)}(\bar{t}_2) &= -\left(\left(\frac{\bar{\Omega}_z}{\bar{\omega}_0}\right)\bar{v}_B\cos\big((\pi/2)(\bar{\Omega}_z/\bar{\omega}_0)\big) - \bar{v}_B\right)\sin\big(2\pi(\bar{\Omega}_z/\bar{\omega}_0)\big) \\
&- \left(\frac{\bar{\Omega}_z}{\bar{\omega}_0}\right)\bar{v}_B\sin\big((\pi/2)(\bar{\Omega}_z/\bar{\omega}_0)\big)\cos\big(2\pi(\bar{\Omega}_z/\bar{\omega}_0)\big) \\
\dot{\bar{z}}_{11}^{(4)}(\bar{t}_2) = \dot{\bar{z}}_{12}^{(4)}(\bar{t}_2) &= 0
\end{aligned}
$$

and for the clouds in the bottom interferometer (21 and 22) we have,

$$
\begin{aligned}
\bar{x}_{21}^{(4)}(\bar{t}_2) = \bar{x}_{22}^{(4)}(\bar{t}_2) &= \frac{\bar{v}_B}{\bar{\omega}_0}\sin\big((\pi/2)(\bar{\Omega}_z/\bar{\omega}_0)\big)\cos\big(2\pi(\bar{\Omega}_z/\bar{\omega}_0)\big) \\
&+ \frac{\bar{v}_B}{\bar{\omega}_0}\cos\big((\pi/2)(\bar{\Omega}_z/\bar{\omega}_0)\big)\sin\big(2\pi(\bar{\Omega}_z/\bar{\omega}_0)\big) \\
\bar{y}_{21}^{(4)}(\bar{t}_2) = \bar{y}_{22}^{(4)}(\bar{t}_2) &= -\frac{\bar{v}_B}{\bar{\omega}_0}\sin\big((\pi/2)(\bar{\Omega}_z/\bar{\omega}_0)\big)\sin\big(2\pi(\bar{\Omega}_z/\bar{\omega}_0)\big) \\
&+ \frac{\bar{v}_B}{\bar{\omega}_0}\cos\big((\pi/2)(\bar{\Omega}_z/\bar{\omega}_0)\big)\cos\big(2\pi(\bar{\Omega}_z/\bar{\omega}_0)\big) \\
\bar{z}_{21}^{(4)}(\bar{t}_2) = \bar{z}_{22}^{(4)}(\bar{t}_2) &= 0 \\
\dot{\bar{x}}_{12}^{(4)}(\bar{t}_2) &= -\left(\frac{\bar{\Omega}_z}{\bar{\omega}_0}\right)\bar{v}_B\sin\big((\pi/2)(\bar{\Omega}_z/\bar{\omega}_0)\big)\sin\big(2\pi(\bar{\Omega}_z/\bar{\omega}_0)\big) \\
&+ \left(\left(\frac{\bar{\Omega}_z}{\bar{\omega}_0}\right)\bar{v}_B\cos\big((\pi/2)(\bar{\Omega}_z/\bar{\omega}_0)\big) - \bar{v}_B\right)\cos\big(2\pi(\bar{\Omega}_z/\bar{\omega}_0)\big) \\
\dot{\bar{x}}_{22}^{(4)}(\bar{t}_2) &= -\left(\frac{\bar{\Omega}_z}{\bar{\omega}_0}\right)\bar{v}_B\sin\big((\pi/2)(\bar{\Omega}_z/\bar{\omega}_0)\big)\sin\big(2\pi(\bar{\Omega}_z/\bar{\omega}_0)\big) \\
&+ \left(\left(\frac{\bar{\Omega}_z}{\bar{\omega}_0}\right)\bar{v}_B\cos\big((\pi/2)(\bar{\Omega}_z/\bar{\omega}_0)\big) + \bar{v}_B\right)\cos\big(2\pi(\bar{\Omega}_z/\bar{\omega}_0)\big) \\
\dot{\bar{y}}_{21}^{(4)}(\bar{t}_2) &= \left(\left(\frac{\bar{\Omega}_z}{\bar{\omega}_0}\right)\bar{v}_B\cos\big((\pi/2)(\bar{\Omega}_z/\bar{\omega}_0)\big) - \bar{v}_B\right)\sin\big(2\pi(\bar{\Omega}_z/\bar{\omega}_0)\big) \\
&+ \left(\frac{\bar{\Omega}_z}{\bar{\omega}_0}\right)\bar{v}_B\sin\big((\pi/2)(\bar{\Omega}_z/\bar{\omega}_0)\big)\cos\big(2\pi(\bar{\Omega}_z/\bar{\omega}_0)\big) \\
\dot{\bar{y}}_{22}^{(4)}(\bar{t}_2) &= \left(\left(\frac{\bar{\Omega}_z}{\bar{\omega}_0}\right)\bar{v}_B\cos\big((\pi/2)(\bar{\Omega}_z/\bar{\omega}_0)\big) + \bar{v}_B\right)\sin\big(2\pi(\bar{\Omega}_z/\bar{\omega}_0)\big) \\
&+ \left(\frac{\bar{\Omega}_z}{\bar{\omega}_0}\right)\bar{v}_B\sin\big((\pi/2)(\bar{\Omega}_z/\bar{\omega}_0)\big)\cos\big(2\pi(\bar{\Omega}_z/\bar{\omega}_0)\big) \\
\dot{\bar{z}}_{21}^{(4)}(\bar{t}_2) = \dot{\bar{z}}_{22}^{(4)}(\bar{t}_2) &= 0
\end{aligned}
$$

The above equations give the position coordinates and velocity components for the four clouds at the moment ($\bar{t} = \bar{t}_2$) of the final split when interactions between different clouds can be neglected. The width equations must be integrated numerically but there are only two distinct widths. In the four–cloud model these are

$$w_{11x}(t) = w_{12x}(t) = w_{11y}(t) = w_{12y}(t) \equiv w_\perp(t)$$

$$\dot{w}_{11x}(t) = \dot{w}_{12x}(t) = \dot{w}_{11y}(t) = \dot{w}_{12y}(t) \equiv \dot{w}_\perp(t)$$

Also, the z widths and dot widths of the two clouds are equal

$$w_{11z}(t) = w_{12z}(t) \equiv w_z(t), \quad \text{and} \quad \dot{w}_{11z}(t) = \dot{w}_{12z}(t) \equiv \dot{w}_z(t)$$

We can also determine the remaining variational parameters for the j^{th} cloud, $\bar{\epsilon}_{j\eta}$ and $\bar{\beta}_{j\eta}$. With these expressions for our variational parameters at time $\bar{t} = \bar{t}_2$ we can determine the M_x, M_y,

and M_z factors appearing in the expression for S_+.

Using the analytical solutions of the cloud–center equations of motion and the symmetries of the solutions of the width equations of motion we can follows the steps of the UVa AI sequence to obtain an analytical expression for $S_+(\Omega_z)$. The result (in SI units) is

$$\begin{aligned} S_+(\Omega_z) &= \frac{1}{2} + \frac{1}{2}\exp\left\{-\left(\frac{2Mv_Bw_\perp}{\hbar}\right)^2 \sin^2\left(\pi\frac{\Omega_z}{\omega_0}\right)\right\} \\ &\times \cos\left\{\left(\frac{2Mv_B^2}{\hbar\omega_0}\right)\left(\sin\left(\tfrac{5\pi}{2}\tfrac{\Omega_z}{\omega_0}\right) - \sin\left(\tfrac{\pi}{2}\tfrac{\Omega_z}{\omega_0}\right)\right)\right\} \end{aligned} \tag{84}$$

and the expression for $S_-(\Omega_z)$ is identical. In the above $w_\perp = w_{jx}(t_2) = w_{jy}(t_2)$ is the transverse width of the condensate at the moment of the final split.

If we observe this in the limit where the rotation speed is much smaller than the trap frequency, $\Omega_z \ll \omega_0$ and hence $\sin\left(a\frac{\Omega_z}{\omega_0}\right) \approx a\frac{\Omega_z}{\omega_0}$, the expression approximates to

$$S_+(\Omega_z) = \frac{1}{2} + \frac{1}{2}\exp\left\{-\left(\frac{2\pi Mv_Bw_\perp}{\hbar\omega_0}\right)^2 \Omega_z^2\right\}\cos\left\{\left(\frac{4M\pi(v_B/\omega_0)^2\Omega_z}{\hbar}\right)\right\} \tag{85}$$

In the case of a harmonic potential the radius of the circular orbit is $R = v_B/\omega_0$ and the area of the orbit is $A = \pi R^2 = \pi(v_B/\omega_0)^2$. With this, we can recognize the argument of the cosine above as the Sagnac phase for a single interferometer:

$$\Phi_S = \frac{4M\pi(v_B/\omega_0)^2\Omega_z}{\hbar} = \frac{4MA\Omega_z}{\hbar}.$$

Furthermore, if we also assume that

$$-\left(\frac{2\pi Mv_Bw_\perp}{\hbar}\right)^2 (\frac{\Omega_z}{\omega_0}^2) << 1 \quad \text{then} \quad \exp\left\{-\left(\frac{2\pi Mv_Bw_\perp}{\hbar\omega_0}\right)^2 \Omega_z^2\right\} \approx 1$$

and then the approximation for S_+ simplifies to,

$$S_+ \approx \frac{1}{2} + \frac{1}{2}\cos(\Phi_S)$$

or

$$S_+ \approx \cos^2(\frac{\Phi_S}{2})$$

which is precisely the result obtained from computing the Sagnac phase from the action integral over the classical path.

The expression for $S_+(\Omega_z)$ in Eq. (85) provides guidance for simulations where inter–cloud interactions and anharmonic terms in the potential are included.

5 Simulations and Results

We investigated the effects of anharmonicity and interactions on the experimental AI sequence by simulating the interferometer experiment for various conditions and then computing the dependence of S_+ on the true rotation speed, Ω_z. The conditions explored included: harmonic and anharmonic potentials, the presence of cloud-cloud interactions, and varying the strength of the interaction by changing the number of condensate atoms. The number of condensate atoms ranged ranged from $N_{\text{atoms}} = 1 \times 10^4$ to 1×10^6 in increments of 1×10^4, and additionally 2×10^6. Note that in all cases self–interactions were present. In total this gives 48 unique combinations of potential, interactions, and number of atoms for which to specify the conditions of the experiment. For each of these 48 combinations we simulated the interferometer experiment at 26 different input rotation speeds at equal intervals ranging from zero up to 125 times the Earth's rotation speed. The values of S_+ were then plotted versus Ω_z for each case. All other parameter values were taken from the original experiment described in section 3.

Initially we investigated the original methodology used by the experimentalists to extract the rotation speed. Namely that the phase accumulated by a cloud is equal to the action along the classical path which yields an equivalence between the fraction of stopped atoms and the squared cosine of half the Sagnac phase. In these simulations we input a "true" rotation speed and then determine a "measured" rotation speed by calculating S–plus with the model and then using the original method. It's worth re-iterating here that this method of reducing the phase to the action along the classical path treats the condensates as point masses and will not account for finite size effects. These "measured" values are then plotted against the "true" rotation speed values for a range from $0 \leq \Omega_{true} \leq 50\Omega_E$ (Ω_E = Earth rotation speed), shown below

The disagreement between the "measured" rotation speed and the "true" rotation speed is significant as the "true" rotation speed approaches zero and is magnified in the case of anharmonicity. This indicates that the method of computing the rotation speed from the Sagnac phase is inaccurate at low rotation speeds and the procedure needs to be modified.

We plotted S–plus versus Ω_{true} for 26 different input rotation speeds at equal intervals from $0 \leq \Omega_{true} \leq 125$ for each of the 48 combinations discussed above. The plots were fit to a function which has the same dependence on Ω_z as the expression for S_+ in Eq. (85) for the case of a harmonic potential and no cloud–cloud interactions. The fit function was

$$S_+(a, b, c, \Omega_z) = \frac{1}{2} + ae^{-b\Omega_z^2} \cos(2\pi c\Omega_z). \tag{86}$$

The fits were performed for data where the rotation speeds were expressed in Hertz. Thus the

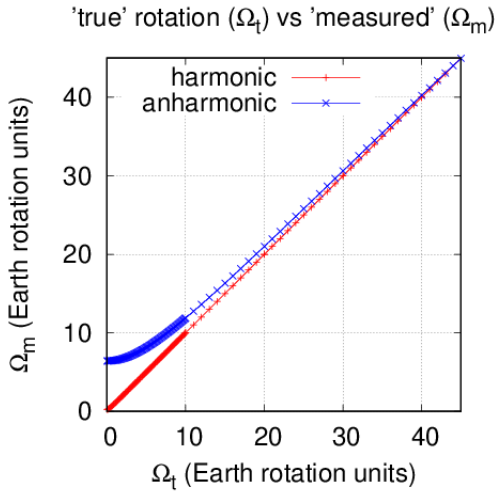

Figure 2: A plot of the "measured" rotation speed versus the "true" rotation speed for harmonic and anharmonic potentials with no interactions present. The values agree well starting around $20\Omega_E$; but as the "true" rotation speed approaches zero, the "measured" and "true" rotation speeds disagree considerably. This is more present in the anharmonic case, but a similar behavior occurs below $1\Omega_E$ for the harmonic case as well.

b parameter is measured in seconds squared and the c parameter is measured in seconds.

Plots of S_+ versus Ω_z for $N_{\text{atoms}} = 10{,}000$ atoms are shown in Figs. 3 and 4 and for $N_{\text{atoms}} = 1{,}000{,}000$ atoms in Figs. 5 and 6. The plots found in these figures are for a harmonic potential with cloud–cloud interactions turned off, harmonic with interactions on, anharmonic with interactions off, and anharmonic with interactions on. These plots also display the values of $S_+(\Omega_z)$ fitted to the function shown in Eq. (86). Note that these fits closely follow the simulation data in all cases.

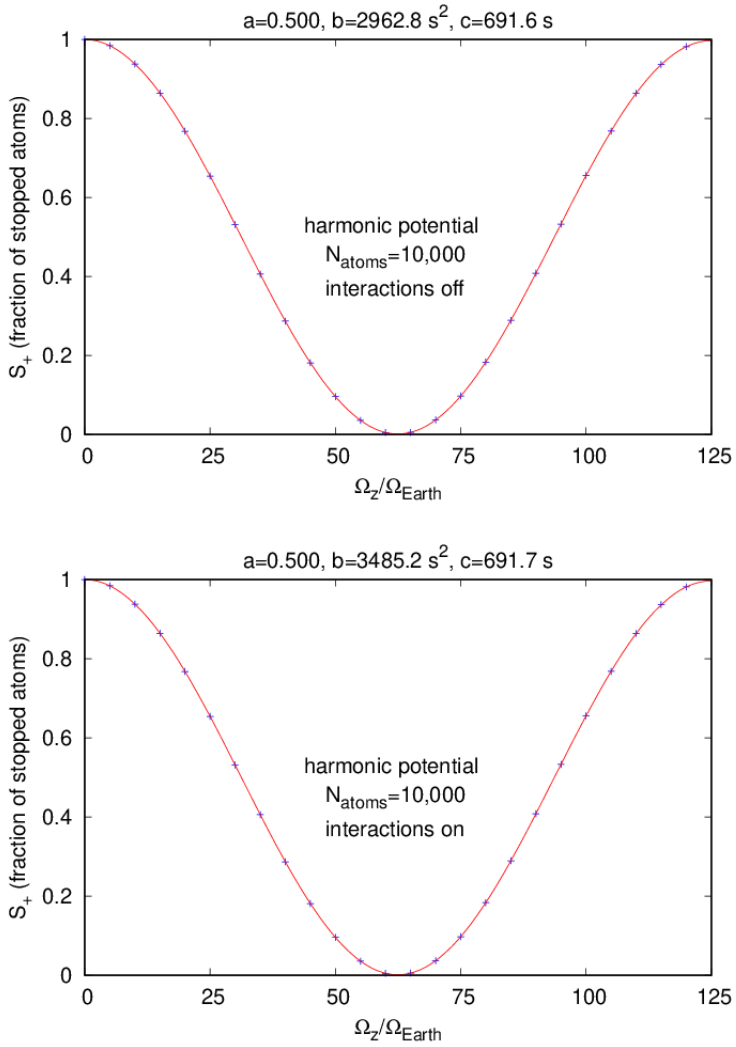

Figure 3: The fraction of stopped atoms, S_+, vs rotating frame speed, Ω_z, with $N_{\rm atoms} = 10{,}000$ ^{87}Rb atoms for the case of a harmonic potential with cloud–cloud interactions off (upper) and on (lower).

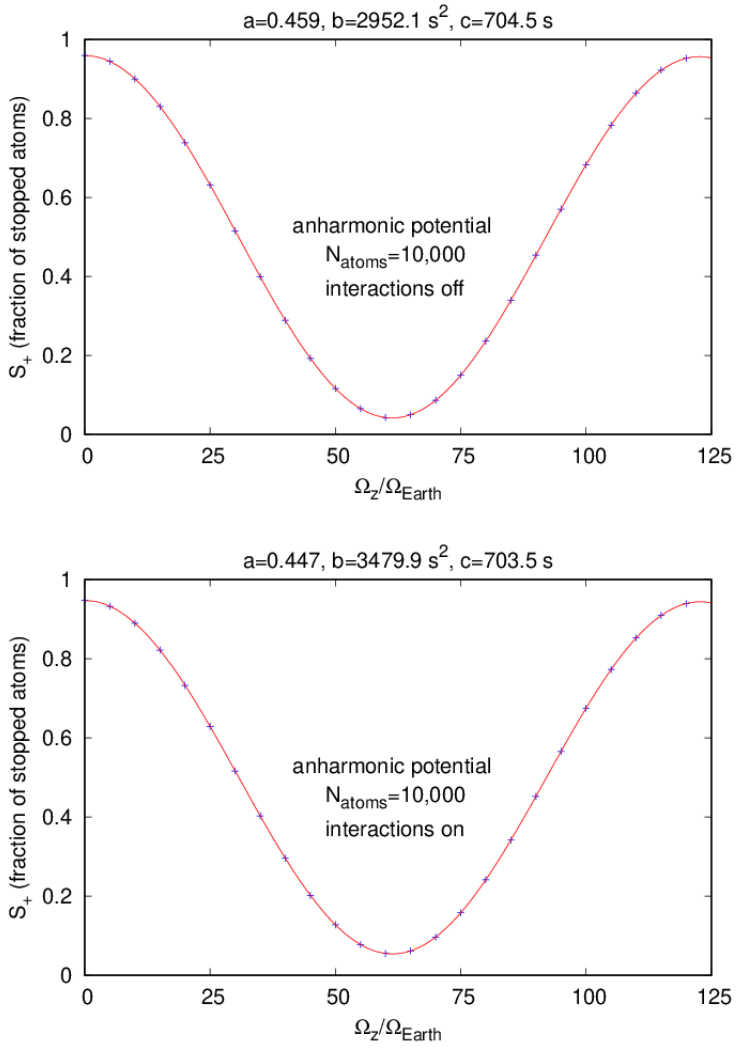

Figure 4: The fraction of stopped atoms, S_+, vs rotating frame speed, Ω_z, with $N_{\rm atoms} = 10{,}000$ ^{87}Rb atoms for the case of an anharmonic potential with cloud–cloud interactions off (upper) and on (lower).

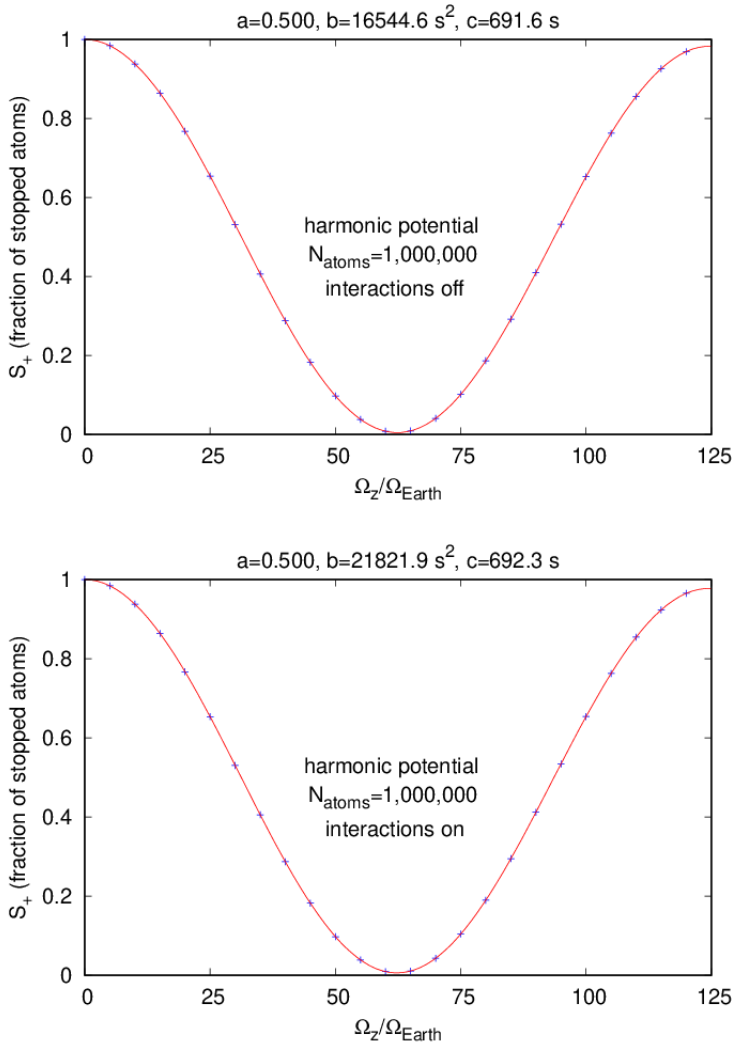

Figure 5: The fraction of stopped atoms, S_+, vs rotating frame speed, Ω_z, with $N_{\rm atoms}$ =1,000,000 ^{87}Rb atoms for the case of a harmonic potential with cloud–cloud interactions off (upper) and on (lower).

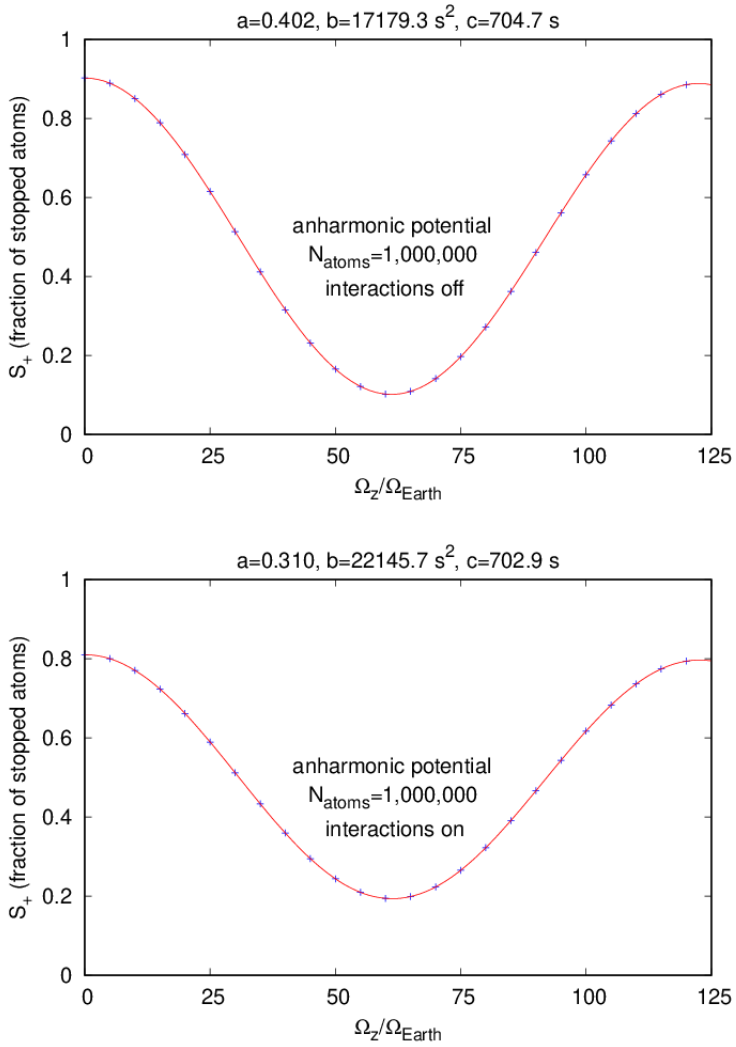

Figure 6: The fraction of stopped atoms, S_+, vs rotating frame speed, Ω_z, with $N_{\rm atoms}$ =1,000,000 ^{87}Rb atoms for the case of an anharmonic potential with cloud–cloud interactions off (upper) and on (lower).

When $\Omega_z = 0$, the above expression becomes $S_+(0) = 1/2 + a$, and comparing this with Eq. (76) we get an approximate formula for a

$$a \approx \tfrac{1}{2}\exp\left\{-\left(\frac{M}{\hbar}\right)^2\left[\tfrac{1}{2}\big(2v_B - (\dot{x}_1 - \dot{x}_2)\big)w_\perp + (x_1 - x_2)\dot{w}_\perp\right]^2 - \left(\frac{x_1^2}{2w_\perp^2} + \frac{x_2^2}{2w_\perp^2}\right)\right\}. \quad (87)$$

the clouds will perfectly overlap when the term in the exponential is zero. This occurs when the width of the condensate is zero, $w_\perp = 0$ and the condensate is treated as a point mass. More importantly, perfect overlap occurs if the relative velocity of the two clouds is $2v_B$, that is $\dot{x}_1 - \dot{x}_2 = 2v_B$ and the centers of the clouds are the same, namely $x_1 - x_2 = 0$. If the cloud centers were different then a relative velocity is still present due to the expansion or contraction of self–interacting clouds. These inferences imply the term a accounts for the finite size of the condensate.

Comparing the fit function with Eq. (85) gives an approximate expression for the b and c parameters, for b we have

$$b \approx \left(\frac{4\pi^2 M v_B}{\hbar\omega_0}\right)^2 w_\perp^2 \quad (88)$$

where we note that this equation gives the value of b when the Ω_z appearing in the exponential is measured in Hz. Here again we see that the term b is indicative of a finite size effect as it depends on $w_\perp^2$. It's also worth noting that b increases for larger rotation speeds and interferometer areas.

From these expressions for a and b we can see that the width of the clouds, $w_\perp$, and to a lesser extent the width velocity, $\dot{w}_\perp$, at the final split have a major effect on the value of S_+.

The c parameter can be approximated by assuming that the quantity appearing in the cosine term is the Sagnac phase. Since the full potential including the anharmonic terms has cylindrical symmetry, the z component of the angular momentum of each cloud is conserved. Thus, if Ω_z in the $\cos(2\pi c\Omega_z)$ factor in Eq. (86) is measured in Hz, we have

$$\begin{aligned} c &= \frac{1}{\hbar}\int_{t_i}^{t_f} dt\,(L_{2z}(t) - L_{1z}(t)) = (L_{2z}(t_f) - L_{1z}(t_f))\int_{t_i}^{t_f} dt \\ c &\approx \left(\frac{M(t_f - t_i)}{\hbar}\right)((x_2\dot{y}_2 - y_2\dot{x}_2) - (x_1\dot{y}_1 - y_1\dot{x}_1))\,. \end{aligned} \quad (89)$$

In the last expression all quantities are evaluated at time $t = t_2$. Below, the values of a, b, and c given by these approximate formulas are compared with their values determined from the simulation fits.

One noticeable feature of these plots is the effect of the anharmonic potential. For the harmonic case, S_+ varies between approximately 0 and 1; however in the anharmonic case, the variation is reduced. Another smaller effect is that the envelope of the variation of S_+ decreases more

rapidly for the anharmonic potential.

The physical mechanisms for these effects can be identified quantitatively by looking at the data found in Tables 1, 2, 3, and 4. These tables compare the values of the fit parameters a, b, and c as determined by the fits with their values calculated from Eqs. (87), (88), and (89) for 12 different condensate numbers. The conditions for Tables 1 - 4 are as follows (in order): harmonic potential with cloud–cloud interactions off, anharmonic potential with interactions off, harmonic potential with interactions on, and anharmonic potential with interactions on.

N_{atoms}	a	a	b (s^2)	b (s^2)	c (s)	c (s)
	(formula)	(fit)	(formula)	(fit)	(formula)	(fit)
10000	0.500	0.500	2962.6	2962.8	691.6	691.6
100000	0.500	0.500	6733.3	6733.6	691.6	691.6
200000	0.500	0.500	8787.9	8788.3	691.6	691.6
300000	0.500	0.500	10291.8	10292.3	691.6	691.6
400000	0.500	0.500	11520.6	11521.1	691.6	691.6
500000	0.500	0.500	12577.9	12578.5	691.6	691.6
600000	0.500	0.500	13515.8	13516.4	691.6	691.6
700000	0.500	0.500	14364.6	14365.2	691.6	691.6
800000	0.500	0.500	15144.0	15144.6	691.6	691.6
900000	0.500	0.500	15867.2	15867.8	691.6	691.6
1000000	0.500	0.500	16543.9	16544.6	691.6	691.6
2000000	0.500	0.500	21789.6	21790.4	691.6	691.6

Table 1: **h_0_xxx:** Comparison of parameters, a, b, and c determined by simulation fits with their values predicted by Eqs. Conditions are harmonic potential and cloud–cloud interactions off.

N_{atoms}	a	a	b (s^2)	b (s^2)	c (s)	c (s)
	(formula)	(fit)	(formula)	(fit)	(formula)	(fit)
10000	0.459	0.459	3027.2	2952.1	702.9	704.5
100000	0.450	0.450	6984.8	6913.5	702.9	704.5
200000	0.441	0.441	9137.4	9072.4	702.9	704.6
300000	0.434	0.434	10711.0	10648.2	702.9	704.6
400000	0.428	0.428	11996.0	11933.8	702.9	704.6
500000	0.422	0.422	13101.1	13039.0	702.9	704.6
600000	0.418	0.418	14081.2	14018.8	702.9	704.6
700000	0.413	0.413	14968.0	14905.2	702.9	704.6
800000	0.409	0.409	15782.1	15718.6	702.9	704.7
900000	0.406	0.406	16537.4	16473.3	702.9	704.7
1000000	0.402	0.402	17244.1	17179.3	702.9	704.7
2000000	0.376	0.376	22720.7	22648.1	703.0	704.7

Table 2: **a_0_xxx:** Comparison of parameters, a, b, and c determined by simulation fits with their values predicted by Eqs. Conditions are anharmonic potential and cloud–cloud interactions off.

The first thing to note is that the approximate formulas for a, b, and c do a good job in predicting the fitted values for these parameters. This is the case for all conditions considered. The formula values for a and c differ from the fitted values by well under 1% and the largest difference in these values for b is less than 5%. Thus these formulas should provide physical insight into the

N_{atoms}	a	a	b (s^2)	b (s^2)	c (s)	c (s)
	(formula)	(fit)	(formula)	(fit)	(formula)	(fit)
10000	0.500	0.500	3475.6	3485.2	691.7	691.7
100000	0.500	0.500	8499.3	8672.5	691.8	691.9
200000	0.500	0.500	11161.0	11439.9	691.9	691.9
300000	0.500	0.500	13093.8	13456.9	692.0	692.0
400000	0.500	0.500	14666.2	15102.4	692.0	692.1
500000	0.500	0.500	16015.4	16517.2	692.1	692.1
600000	0.500	0.500	17209.5	17771.8	692.1	692.1
700000	0.500	0.500	18288.4	18907.2	692.2	692.2
800000	0.500	0.500	19277.5	19949.5	692.2	692.2
900000	0.500	0.500	20194.3	20916.7	692.2	692.2
1000000	0.500	0.500	21051.2	21821.9	692.2	692.3
2000000	0.500	0.500	27667.0	28842.8	692.2	692.5

Table 3: **h_1_xxx:** Comparison of parameters, a, b, and c determined by simulation fits with their values predicted by Eqs. Conditions are harmonic potential and cloud–cloud interactions on.

N_{atoms}	a	a	b (s^2)	b (s^2)	c (s)	c (s)
	(formula)	(fit)	(formula)	(fit)	(formula)	(fit)
10000	0.447	0.447	3553.9	3479.9	703.0	703.5
100000	0.407	0.407	8718.4	8764.5	703.2	702.6
200000	0.385	0.385	11454.4	11584.0	703.3	702.6
300000	0.370	0.370	13440.9	13637.3	703.4	702.6
400000	0.357	0.357	15056.9	15311.7	703.4	702.7
500000	0.347	0.347	16443.3	16751.0	703.5	702.7
600000	0.338	0.338	17670.5	18027.1	703.5	702.8
700000	0.330	0.330	18779.3	19181.8	703.5	702.8
800000	0.323	0.323	19795.7	20241.7	703.6	702.8
900000	0.316	0.316	20737.8	21225.3	703.6	702.8
1000000	0.310	0.310	21618.4	22145.7	703.6	702.8
2000000	0.268	0.268	28417.3	29283.9	703.9	702.8

Table 4: **a_1_xxx:** Comparison of parameters, a, b, and c determined by simulation fits with their values predicted by Eqs. Conditions are anharmonic potential and cloud–cloud interactions on.

effects of interactions and the anharmonic potential.

The expression for a in Eq. (87) shows that, in order to maximize a at zero rotation speed, the centers of the two clouds must coincide and their relative velocity x components must be $2v_B$ just before the final split. This is more difficult to achieve in the presence of anharmonic terms, as indicated by the comparison tables. The value of b is insensitive to the presence of anharmonic terms in the potential. The striking feature of the variation of b for increasing number of atoms is that its value increases significantly when cloud–cloud interactions are present versus when they are absent. The main driver of this effect occurs at the second split when two clouds become four clouds. Without cloud–cloud interactions, the rate of change of the transverse cloud width ($w_\perp(t_1)$) begins to decrease sharply while this rate of change continues to increase when interactions are present. This leads to a significantly larger value of $w_\perp(t_2)$ at the final

split. The b parameter directly measures an effect of the finite–width of the condensate at the time of the final split as shown in Eq. (88). It is worth noting that its effect on the value of S_+ is increased for larger rotation speed and, importantly, also for larger interferometer areas. It is therefore possible that this effect may need to be accounted for in the data analysis of the experimental results for larger–area interferometers. Another notable feature is that the c parameter is insensitive to the number of condensate atoms. Also the c parameter is larger for the anharmonic potential. This is because the anharmonic potential causes the cloud trajectories to displace out of the xy plane, thus increasing the area enclosed when compared to the harmonic potential. Furthermore, because the fit and formula values for c match well, it shows that the argument, $2\pi c\Omega_z$, is the Sagnac phase.

6 Summary

In this work we investigated a recent dual–Sagnac atom interferometer device using a variational model which provides rapid approximate solutions to the rotating–frame Gross–Pitaevskii equation. This device uses a split Bose–Einstein condensate in an ideally harmonic potential to measure the external rotation speed of the system. We used the model to study the effects of interactions and anharmonicity on the performance of the device. In particular we explored these effects through an increasing number of condensate atoms at various rotation speeds.

We found the presence of interactions to cause variations in the sizes of the condensate clouds. Two forms of interactions were described here, those between the atoms in a cloud (self–interactions) and those between atoms in different clouds (cloud–cloud interactions). In either case the strength of interactions increases with a larger density of atoms present. When a cloud is split into two the repulsive strength is lessened while the confinement from the external potential remains the same. This causes the cloud to contract, increasing the repulsion. Eventually the repulsion is strong enough so they stop contracting and begin to expand. This breathing motion due to self–interactions leads to a change in the cloud's final size. We found that interactions between different clouds can moderate the change in the rate of oscillation when a cloud is split. This allows one to minimize the final width by modifying the four–cloud flight time. We also found that the finite size of the condensate caused a slow decay in the envelope of the variation of the stopped–atom fraction, $S_\pm$, with increasing rotating–frame speed, Ω_z. This is demonstrated by parameter b in the study. The rate of decay is proportional to the square of the condensate width at the final split. The decay rate is also proportional to the interferometer area. We expect the effects of interactions to be important in state–of–the–art interferometer applications.

Our model shows that the presence of anharmonic terms in the potential cause the amplitude of the envelope of the variation of the stopped–atom fraction. This is due to a relative velocity between overlapping clouds and/or a lack of complete spatial overlap at the final split, see parameter a in the study. The anharmonic terms in general will not affect the clouds in an interferometer the same and cause the clouds to develop a relative velocity between them. This can be a combination of the relative velocity of the cloud centers and the expansion or contraction of the clouds; hence these effects decrease when the final width decreases. The trapping potential can be engineered so as to minimize these effects to ensure a strong output signal, a necessity for sensitive measurements.

The model also predicts that the frequency of the variation of the stopped–atom fraction depends on the Sagnac phase regardless of the presence of interactions and/or anharmonicity, as indicated by parameter c in the study. In all cases $S_{\pm}$ varied sinusoidally with the Sagnac phase. This is critical for the performance of the device. It also suggests that the fit function, Eq. (86), could be used to construct a similar procedure to the ellipse–fitting analysis used in the experiment. One which allows for common–mode rejections but accounts for interactions and anharmonic effects.

References

[1] K. Bongs, M. Holynski, J. Vovrosh, P. Bouyer, G. Condon, E. Rasel, C. Schubert, W. P. Schleich, and A. Roura, *Taking atom interferometric quantum sensors from the laboratory to real-world applications*, Nature Reviews Physics **1**, 731 (2019).

[2] G. Geneves, P. Gournay, A. Gosset, M. Lecollinet, F. Villar, P. Pinot, P. Juncar, A. Clairon, A. Landragin, D. Holleville, F. P. Dos Santos, J. David, M. Besbes, F. Alves, L. Chassagne, and S. Topcu, *The BNM Watt balance project*, IEEE Transactions on Instrumentation and Measurement **54**, 850 (2005).

[3] H. P. Richard, C. Yu, W. Zhong, B. Estey, and H. Maller, *Measurement of the fine-structure constant as a test of the standard model*, Science **360**, 6385 (2018).

[4] G. Rosi, F. Sorrentino, L. Cacciapuoti, M. Prevedelli, and G. M. Tino, *Precision measurement of the Newtonian gravitational constant using cold atoms*, Nature **510** (2014).

[5] V. Ménoret, P. Vermeulen, N. Le Moigne, S. Bonvalot, P. Bouyer, A. Landragin, and B. Desruelle, *Gravity measurements below* $10^{-9}\,g$ *with a transportable absolute quantum gravimeter*, Scientific Reports **8**, 12300 (2018).

[6] D. S. Weiss, B. C. Young, and S. Chu, *Precision measurement of the photon recoil of an atom using atomic interferometry*, Phys. Rev. Lett. **70**, 2706 (1993).

[7] B. Andreas et al., *Determination of the Avogadro Constant by Counting the Atoms in a* ^{28}Si *Crystal*, Phys. Rev. Lett. **106**, 030801 (2011).

[8] R. Bouchendira, P. Cladé, S. Guellati-Khélifa, F. m. c. Nez, and F. m. c. Biraben, *New Determination of the Fine Structure Constant and Test of the Quantum Electrodynamics*, Phys. Rev. Lett. **106**, 080801 (2011).

[9] D. Hanneke, S. Fogwell, and G. Gabrielse, *New Measurement of the Electron Magnetic Moment and the Fine Structure Constant*, Phys. Rev. Lett. **100**, 120801 (2008).

[10] J. B. Fixler, G. T. Foster, J. M. McGuirk, and M. A. Kasevich, *Atom interferometer measurement of the Newtonian constant of gravity*, Science **315**, 74 (2007).

[11] A. Bonnin, N. Zahzam, Y. Bidel, and A. Bresson, *Simultaneous dual-species matter-wave accelerometer*, Phys. Rev. A **88**, 043615 (2013).

[12] S. Dimopoulos, P. W. Graham, J. M. Hogan, M. A. Kasevich, and S. Rajendran, *Atomic gravitational wave interferometric sensor*, Phys. Rev. D **78**, 122002 (2008).

[13] J. M. Hogan and M. A. Kasevich, *Atom-interferometric gravitational-wave detection using heterodyne laser links*, Phys. Rev. A **94**, 033632 (2016).

[14] J. M. Hogan, D. M. S. Johnson, S. Dickerson, T. Kovachy, A. Sugarbaker, S.-w. Chiow, P. W. Graham, M. A. Kasevich, B. Saif, S. Rajendran, P. Bouyer, B. D. Seery, L. Feinberg, and R. Keski-Kuha, *An atomic gravitational wave interferometric sensor in low earth orbit (AGIS-LEO)*, General Relativity and Gravitation **43**, 1953 (2011).

[15] S. M. Dickerson, J. M. Hogan, A. Sugarbaker, D. M. S. Johnson, and M. A. Kasevich, *Multiaxis Inertial Sensing with Long-Time Point Source Atom Interferometry*, Phys. Rev. Lett. **111**, 083001 (2013).

[16] L. Zhou, Z. Xiong, W. Yang, B. Tang, W. Peng, K. Hao, R. Li, M. Liu, J. L. Wang, and M. Zhan, *Development of an atom gravimeter and status of the 10-meter atom interferometer for precision gravity measurement*, General Relativity and Gravitation **43**, 1931 (2011).

[17] B. Barrett, L. Antoni-Micollier, L. Chichet, B. Battelier, T. Lévèque, A. Landragin, and P. Bouyer, *Dual matter-wave inertial sensors in weightlessness*, Nature Communications **7**, 13786 (2016).

[18] C. Antoine and C. J. Bord, *Quantum theory of atomic clocks and gravito-inertial sensors: an update*, Journal of Optics B: Quantum and Semiclassical Optics **5**, S199 (2003).

[19] R. Geiger, V. Ménoret, G. Stern, N. Zahzam, P. Cheinet, B. Battelier, A. Villing, F. Moron, M. Lours, Y. Bidel, A. Bresson, A. Landragin, and P. Bouyer, *Detecting inertial effects with airborne matter-wave interferometry*, Nature Communications **2**, 474 (2011).

[20] P. Amaro-Seoane et al., *Low-frequency gravitational-wave science with eLISA/NGO*, Classical and Quantum Gravity **29**, 124016 (2012).

[21] W. Chaibi, R. Geiger, B. Canuel, A. Bertoldi, A. Landragin, and P. Bouyer, *Low frequency gravitational wave detection with ground-based atom interferometer arrays*, Phys. Rev. D **93**, 021101 (2016).

[22] E. R. Moan, R. A. Horne, T. Arpornthip, Z. Luo, A. J. Fallon, S. J. Berl, and C. A. Sackett, *Quantum Rotation Sensing with Dual Sagnac Interferometers in an Atom-Optical Waveguide*, Phys. Rev. Lett. **124**, 120403 (2020).

[23] T. M. Niebauer, M. P. McHugh, and J. E. Faller, *Galilean test for the fifth force*, Phys. Rev. Lett. **59**, 609 (1987).

[24] P. Touboul et al., *MICROSCOPE Mission: First Results of a Space Test of the Equivalence Principle*, Phys. Rev. Lett. **119**, 231101 (2017).

[25] Z. Zhang, V. Dunjko, and M. Olshanii, *Atom transistor from the point of view of nonequilibrium dynamics*, New Journal of Physics **17**, 125008 (2015).

[26] S. Fray, C. A. Diez, T. W. Hänsch, and M. Weitz, *Atomic Interferometer with Amplitude Gratings of Light and Its Applications to Atom Based Tests of the Equivalence Principle*, Phys. Rev. Lett. **93**, 240404 (2004).

[27] M. G. Tarallo, T. Mazzoni, N. Poli, D. V. Sutyrin, X. Zhang, and G. M. Tino, *Test of Einstein Equivalence Principle for 0-Spin and Half-Integer-Spin Atoms: Search for Spin-Gravity Coupling Effects*, Phys. Rev. Lett. **113**, 023005 (2014).

[28] D. Schlippert, J. Hartwig, H. Albers, L. L. Richardson, C. Schubert, A. Roura, W. P. Schleich, W. Ertmer, and E. M. Rasel, *Quantum Test of the Universality of Free Fall*, Phys. Rev. Lett. **112**, 203002 (2014).

[29] G. Rosi, *A proposed atom interferometry determination of G at 10-5 using a cold atomic fountain*, Metrologia **55**, 50 (2017).

[30] G. Rosi, G. D'Amico, L. Cacciapuoti, F. Sorrentino, M. Prevedelli, M. Zych, Č. Brukner, and G. M. Tino, *Quantum test of the equivalence principle for atoms in coherent superposition of internal energy states*, Nature Communications **8**, 15529 (2017).

[31] R. Geiger and M. Trupke, *Proposal for a Quantum Test of the Weak Equivalence Principle with Entangled Atomic Species*, Phys. Rev. Lett. **120**, 043602 (2018).

[32] B. Elder, J. Khoury, P. Haslinger, M. Jaffe, H. Müller, and P. Hamilton, *Chameleon dark energy and atom interferometry*, Phys. Rev. D **94**, 044051 (2016).

[33] P. Hamilton, M. Jaffe, P. Haslinger, Q. Simmons, H. Müller, and J. Khoury, *Atom-interferometry constraints on dark energy*, Science **349**, 849 (2015).

[34] M. Jaffe, P. Haslinger, V. Xu, P. Hamilton, A. Upadhye, B. Elder, J. Khoury, and H. Müller, *Testing sub-gravitational forces on atoms from a miniature in-vacuum source mass*, Nature Physics **13**, 938 (2017).

[35] L. E. Strigari, *Galactic searches for dark matter*, Physics Reports **531**, 1 (2013).

[36] A. Arvanitaki, P. W. Graham, J. M. Hogan, S. Rajendran, and K. Van Tilburg, *Search for light scalar dark matter with atomic gravitational wave detectors*, Phys. Rev. D **97**, 075020 (2018).

[37] A. Hees, J. Guéna, M. Abgrall, S. Bize, and P. Wolf, *Searching for an Oscillating Massive Scalar Field as a Dark Matter Candidate Using Atomic Hyperfine Frequency Comparisons*, Phys. Rev. Lett. **117**, 061301 (2016).

[38] C. Overstreet, P. Asenbaum, T. Kovachy, R. Notermans, J. M. Hogan, and M. A. Kasevich, *Effective Inertial Frame in an Atom Interferometric Test of the Equivalence Principle*, Phys. Rev. Lett. **120**, 183604 (2018).

[39] E. Moan, S. Berl, Z. Luo, and C. A. Sackett, Controlling the anharmonicity of a time-orbiting potential trap, in *Optical, Opto-Atomic, and Entanglement-Enhanced Precision Metrology II*, edited by S. M. Shahriar and J. Scheuer, Vol. 11296, p. 238–245, International Society for Optics and Photonics, SPIE, 2020.

[40] R. A. Horne and C. A. Sackett, *A cylindrically symmetric magnetic trap for compact Bose-Einstein condensate atom interferometer gyroscopes*, Review of Scientific Instruments **88**, 013102 (2017).

[41] K. J. Hughes, B. Deissler, J. H. T. Burke, and C. A. Sackett, *High-fidelity manipulation of a Bose-Einstein condensate using an optical standing wave*, Phys. Rev. A **76**, 035601 (2007).

[42] O. Garcia, B. Deissler, K. J. Hughes, J. M. Reeves, and C. A. Sackett, *Bose-Einstein-condensate interferometer with macroscopic arm separation*, Phys. Rev. A **74**, 031601 (2006).

[43] C. Pethick and H. Smith, *Bose-Einstein condensation in dilute gases*, Cambridge University Press, 2002.

[44] Y.-J. Wang, D. Z. Anderson, V. M. Bright, E. A. Cornell, Q. Diot, T. Kishimoto, M. Prentiss, R. A. Saravanan, S. R. Segal, and S. Wu, *Atom Michelson Interferometer on a Chip Using a Bose-Einstein Condensate*, Phys. Rev. Lett. **94**, 090405 (2005).

[45] E. Moan, Z. Luo, and C. Sackett, A large-area sagnac interferometer using atoms in a time-orbiting potential, in *Optical, Opto-Atomic, and Entanglement-Enhanced Precision Metrology*, Vol. 10934, p. 109341X, International Society for Optics and Photonics, 2019.

[46] E. Majorana, *Atomi orientati in campo magnetico variabile*, Il Nuovo Cimento (1924-1942) **9**, 43 (1932).

[47] Z. Luo, E. Moan, and C. Sackett, *Semiclassical Phase Analysis for a Trapped-Atom Sagnac Interferometer*, Atoms **9**, 21 (2021).

[48] E. Ashwood, E. W. Wells, D. M. Kurkcuoglu, R. C. Sapp, C. W. Clark, and M. Edwards, *Tools for designing atom interferometers in a microgravity environment*, Phys. Rev. A **99**, 043615 (2019).